Flexural Performance of Nail-Laminated Timber Crane Mats

A THESIS
SUBMITTED TO THE FACULTY OF
UNIVERSITY OF MINNESOTA
BY

Ethan L. Herberg

IN PARTIAL FULFILLMENT OF THE REQUIREMENTS
FOR THE DEGREE OF MASTER OF SCIENCE

DR. BENJAMIN Z. DYMOND

December 2018

Acknowledgements

I would like to first thank my advisor Dr. Ben Dymond for his unwavering support and guidance throughout my project. Additionally, I would like to thank my committee members Dr. Andrea Shcokker and Matt Aro for dedicating much of their time and providing critical insight into the topics of my thesis. Without their help and help from the faculty of the University of Minnesota Duluth Civil Engineering Program I could not have completed this project. I would also like to thank my fellow structural graduate students who spent numerous hours assisting me in in the lab and encouraged me constantly.

I am thankful for Savanna Pallets, Inc. of Cloquet, Minnesota and the University of Minnesota Duluth Natural Resources Research Institute for providing specimens and financial support through the NRRI Business Assistance Fund. Furthermore, I would like to thank them for their commitment throughout the different phases of this project and for providing valuable industry perspective.

Finally, I would like to sincerely thank my family and friends for their continuous support throughout my time in college. The confidence and gratitude that they instilled in me enabled me to persevere in my studies and life outside of school. I am very thankful for them and the way they have shaped me to be the person that I am today.

Abstract

A crane mat is a temporary platform used to stabilize heavy equipment and vehicles, while allowing for passage over various ground conditions. Crane mats are typically used as temporary roadways for pipeline installation, oil mining, electric power transmission, and general construction. Traditional designs range from solid timber mats held together with steel bolts to plastic and rubber composite mats. Nail-laminated timber (NLT) is an economically available alternative type of crane mat design. Nail-laminated timber structural elements are created by placing several pieces of dimensional lumber on the thinner edge and fastening the individual laminations together with nails or screws along the wide face of the lumber. Although NLT is an age-old timber construction method, its benefits are being rediscovered as wood technology continues to progress.

This research was conducted in collaboration with Savanna Pallets, Inc. and the University of Minnesota Duluth Natural Resources Research Institute (NRRI) as part of a larger project. Specifically, this research had three specific goals. The first was to evaluate if NLT can be effectively manufactured using underutilized, small diameter, local wood species in collaboration with Savanna Pallets, Inc. Each specimen was fabricated with various fastener types, fastener spacing patterns, joint locations, and moisture contents. Through a series of design phases, it was determined that NLT can successfully be manufactured by fastening low grade lumber with either nails, screws or scrails.

The second goal was to experimentally determine the NLT crane mat flexural performance and compare the results to current design recommendations for structural applications. Each specimen was tested to determine the maximum applied load, corresponding deflection, and modulus of elasticity (MOE) when subjected to static bending. The Nail-laminated Timber Design Guide (2017) and the International Building Code (2018) were used for theoretical predictions because there are currently no standards or specifications for crane mat design using NLT. The theoretical predictions for flexural strength, deflection at the maximum applied load, and MOE were typically conservative when compared to the experimentally measured values.

The third goal was to determine the specific lumber and fastener configuration that produced a finished product which was economical for Savanna Pallets, Inc. The experimental test results suggested that a random distribution of butt joints in individual

laminations of lumber yielded a greater flexural strength than butt joints placed in an organized, symmetric fashion. Furthermore, NLT specimens fastener together with multi-purpose framing screws exhibited the highest flexural strength and largest deflection at the maximum applied load out of the three types of fasteners. The experimentally measured MOE was similar between the three fastener types, but much lower for specimens constructed with a symmetric layup compared to specimens constructed with butt joints in a randomized pattern. Additional research with a larger sample size for each unique design is recommended to better understand the flexural behavior of NLT crane mats constructed with low grade lumber.

TABLE OF CONTENTS

LIST OF TABLES

LIST OF FIGURES

NOTATION

b_{panel}	=	NLT panel width (in.)
C_D	=	load duration factor
C_F	=	size factor for sawn lumber
C_{fu}	=	flat use factor
C_i	=	incising factor for dimensional lumber
C_L	=	beam stability factor
C_M	=	wet service factor
C_r	=	repetitive member factor for dimensional lumber, prefabricated wood I-joists, and structural composite lumber
C_t	=	temperature factor
d	=	NLT depth (in.)
E	=	reference modulus of elasticity (psi)
E_{NLT}'	=	NLT modulus of elasticity (psi)
E'	=	modulus of elasticity adjusted by applicable factors (psi)
EI	=	Bending stiffness of NLT ($lb*in^2$)
F_b	=	reference bending design value (psi)
f_b	=	actual bending stress (psi)
F_b'	=	adjusted bending design value (psi)
$F_{b.NLT}'$	=	NLT bending capacity (psi)
FS	=	factor of safety
I	=	moment of inertia ($in.^4$)
$K_{layup.b}$	=	layup factor for bending strength
$K_{layup.E}$	=	layup factor for stiffness
$K_{section.b}$	=	cross section factor for bending strength
$K_{section.E}$	=	cross section factor for stiffness
l	=	span length (in.)
M	=	maximum bending moment (in.-lb)
P	=	maximum allowable point load (lb)
S	=	section modulus ($in.^3$)

s	=	nail spacing in direction of span (in.)
w	=	uniformly distributed live load (lb/in.)
y	=	depth to neutral axis (in.)
Δ	=	deflection (in.)
σ	=	allowable bending stress (psi)
σ_b	=	allowable total area load limited by bending (psi)
σ_P	=	allowable distributed point load (lb/ft)
σ_Δ	=	allowable total area load limited by deflection (psi)

CHAPTER 1. INTRODUCTION

1.1 Background

1.1.1 Crane Mats

A crane mat is a portable platform used to stabilize heavy-equipment and vehicles, while allowing for passage over various ground conditions. Crane mats are often referred to as access mats or swamp mats. Crane mats are used to provide the construction equipment with a solid foundation to rest on in the event that construction must occur in unfavorable terrains that are difficult for cranes and other equipment to navigate. Crane mats are typically used as temporary roadways for pipeline installation, oil mining, electric power transmission, and general construction. A potential use of crane mats during powerline construction is shown in Figure 1.1. Alternatively, they may be used as temporary decking during bridge construction or during disaster relief and environmental remediation (Quality Mat Company, 2018).

Aside from the benefit of being able to withstand heavy loads, crane mats possess a number of other unique advantages. Temporary roads built with these mats promote the communication of job site entry and exit points to contractors and construction crews. Ensuring a clear path of traffic can prevent accidents, delays, and admittance to dangerous locations on the project site. Crane mats can also be used to protect environmentally sensitive landscapes during construction. Operating heavy equipment without the use of mats can result in soil compaction, erosion and even failure. Delicate agriculture and other aspects of the environment can be disrupted during large-scale construction projects, but the use of crane mats can help preserve the surroundings (Spartan Mat, 2018). Due to the ease of fabrication, crane mats can be tailored to meet diverse project requirements. Customizable mat dimensions and lifting options allow for efficient transportation to construction sites and fast placement in the field.

The first crane mat systems were based on a design established in the late 20th century by Joe Penland (Quality Mat Company, 2018). The design consisted of three layers of 2x8 lumber connected with steel bolts. Typically, the top and bottom layers were made of 11 longitudinal pieces of lumber and the middle layer, placed cross-wise, was made of 21 pieces of lumber. In the USA, the majority of crane mats are constructed using mixed

hardwood timber. The hardwood timber is often referred to as oak. Crane mats are mass-produced products and quality varies considerably within the industry. Common mat dimensions include 4 x 16 ft and 8 x 20 ft, with depths that vary between suppliers. Specific applications, dimensions, load capacities, and other required characteristics can be used to determine the most appropriate crane mat. As technology has advanced, a variety of crane mat systems have emerged. This includes, but is not limited to, composite (steel and plastic), steel framed, solid timber, and cross-laminated timber (CLT) mats. Each individual crane mat system is defined based on the material and method of fabrication.

Composite mats are commonly constructed as one of two systems: (1) a solid plastic, one piece compression molded system or (2) an engineered, hollow rig matting system. Both types of composite mat systems are fabricated from new or recycled, high-density polyethylene and feature a variety of connection mechanisms. Mat connections can range from simple interlocking grooves along the perimeter to complicated devices with small parts (Tufftrak Ground Protection Solutions, 2018). Composite mats are typically lighter in weight than traditional crane mats, but they are often not able to maintain their structural integrity under excessive weight. Although composite mats are more expensive upfront, they have a much longer lifespan compared to traditional timber designs (Spartan Mat, 2018). A typical layout of composite mats for an access road is shown in Figure 1.2.

Solid timber mats are typically constructed of 12 x 12 in. timbers and are fastened together with large steel bolts. The most common solid timber mats are made from Douglas-fir or dense hardwood timbers (Sterling, 2018). Steel bolts holding the mat together are cut flush with the edge of the outer most timbers and nuts are countersunk into the side of the mat. The manufacturing process allows for versatility as different lengths and sizes of timbers can be used to create mats of various dimensions. A variety of lifting options including exposed bolts, lift hooks, and chains can be installed to meet specific project needs. A series of solid timber mats supporting a crane is displayed in Figure 1.3.

Steel framed mats are constructed with a combination of steel and wood to endure the heaviest loads from industrial equipment (Northern Mat & Bridge, 2018). The wood component typically consists of many layers of standard lumber and each layer is glued together such that the grain runs parallel with the length of the mat. Encasing the lumber is a steel frame, which is normally made of I-beams or C-channels. A typical steel framed

mat design is shown in Figure 1.4. The steel is used to strengthen the mats and enables the manufacturers to fabricate larger sizes than traditional crane mats. Side beam shackles are often attached at the ends of the member for easy maneuverability. Some steel framed mats may be reinforced with steel plates across the layers of lumber to increase the load carrying capacity of the mat. The greatest advantage of steel framed mats is that steel helps to protect the edges of the lumber. If damaged, the wooden inserts can easily be repaired, renewing the life of the mat (Alberta Rig Mats, 2018).

Cross-laminated timber mats are another common type of crane mat system used in the industry. Cross-laminated timber is a new generation of engineered wood products that has been introduced to building and industrial applications. Cross-laminated timber is a wood panel that is typically made of three, five, or seven layers of dimensional lumber with each layer oriented perpendicular to the adjacent layers. The individual layers are fastened together using glue, nails, or both. A common CLT mat design with exposed bolts for lifting is shown in Figure 1.5. The two-way action of the CLT layers parallel and perpendicular to the span of the member provides more strength and rigidity compared to lumber used in more traditional designs because the load can be distributed in either direction (CLT Handbook, 2013).

1.1.2 Nail-Laminated Timber

Nail-laminated timber (NLT) is an economically available alternative type of crane mat design. Nail-laminated timber structural elements are created by placing several pieces of dimensional lumber on the thinner edge and fastening the individual laminations together with nails or screws along the wide face of the lumber. A depiction of standard edgewise NLT construction is shown in Figure 1.6. Part of the family of mass timber products, NLT is commonly used as floors, roofs, and walls (NLT Design Guide, 2017). Although NLT is an age-old construction method, its benefits are being rediscovered as wood technology continues to advance. The benefits of NLT stem from the fact that timber possesses a high strength-to-weight ratio. In recent years, the percentage of structures built with nail-laminated timber panels has increased at an exceptional rate (NLT Design Guide, 2017). This trend can be attributed to the fact that solid timber elements become considerably more expensive as the required span lengths increase. NLT is advantageous among mass timber products because it does not require a unique manufacturing process

compared to other mass timber products like CLT. Nail-laminated timber is an easily accessible material as it can be fabricated with local dimensional lumber for use in a number of applications (NLT Design Guide, 2017).

Nail-laminated timber is a monolithic slab system that spans in one direction to resist out-of-plane bending. It can be conceptualized structurally as joists spaced at the width of one joist on center (o.c.) (e.g., for 2x material, joists spaced a 1-1/2 in. o.c.). Plywood or oriented strand board (OSB) may be added to one face of an NLT panel to provide in-plane shear capacity, allowing for use in lateral force resisting systems of buildings. Given the efficient load carrying capacity compared to the weight of typical lumber, serviceability requirements such as deflection and vibration often govern the design of NLT used to resist gravity loads.

The ease of construction allows for NLT components to be fabricated with any species, grade, and size of dimensional lumber. Typical dimensional lumber in the USA is milled with slightly rounded corners, giving NLT a distinctive grooved texture. To achieve a smooth face across the entire surface, NLT is assembled and planed or sanded smooth. Nail-laminated timber may be fabricated with butt joints in individual laminations along the length of the span in order to reduce costs. This permits the use of various lengths of lumber to achieve greater spans than traditional designs (NLT Design Guide, 2017).

1.2 Motivation and Objectives

The research described within this document was conducted in collaboration with Savanna Pallets, Inc. and the University of Minnesota Duluth Natural Resources Research Institute (NRRI) as part of a larger project. The experimental testing of the NLT specimens and modulus of elasticity (MOE) samples was conducted in the structures laboratory at the University of Minnesota Duluth (UMD) and the Mechanical Test Laboratory at the NRRI, respectively. This project had three specific goals. The first was to evaluate if NLT panels can be effectively manufactured using underutilized, small diameter, local wood species in collaboration with Savanna Pallets, Inc. The specimens were constructed using low value northern red oak lumber from the Duluth region (e.g., the Chippewa National Forest). The forest resource market in the Duluth area does not currently have a steady need for the underutilized, small diameter timber used to construct the NLT specimens in this study. The timber was sourced from forested lands with high wildfire risk, which in turn could

reduce costs of forest management. The second goal was to experimentally determine the NLT mat flexural strength and MOE and compare the results to current design recommendations for structural applications. The NLT mats were fabricated with various fastener types, fastener spacing patterns, joint locations, and moisture contents. Each specimen was tested to determine the maximum applied point load and corresponding deflection when subjected to static bending. The third goal was to determine the specific lumber and fastener configuration that produced a finished product which was economical for Savanna Pallets, Inc.

1.3 Thesis Organization

Chapter two presents a literature review including current design recommendations for structural applications of NLT and an overview of previous research closely related to this study. Chapter three discusses fabrication of the NLT specimens, and it also includes a description of the test setups and the testing procedures performed in this research. Information describing the instrumentation used during testing is also provided in chapter three. Chapter four presents the experimental results from each test with comparisons to design specifications and a discussion of the data. The final chapter highlights the conclusions from testing, recommendations, and suggested future research.

Figure 1.1. Use of crane mats during powerline construction (© TerraPro, Inc., 2018)

Figure 1.2. Access road constructed with composite mats (© Matrax, Inc., 2018)

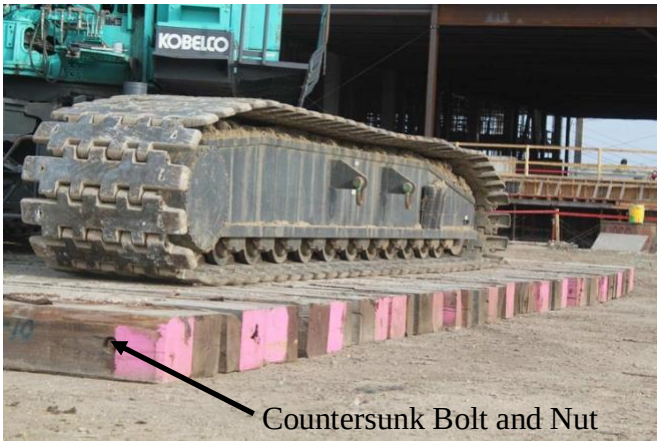

Figure 1.3. Solid timber mats supporting a crane (© Quality Mat Company, 2018)

Figure 1.4. Typical steel framed crane mats (© Matrax, Inc., 2018)

Figure 1.5. Common CLT mat design with exposed bolts for lifting (© Rig Mats of America, Inc., 2018)

Figure 1.6. Edgewise construction of NLT panels (© StructureCraft Builders, Inc., 2018)

CHAPTER 2. LITERATURE REVIEW

2.1 NLT Design

2.1.1 Introduction

Nail-laminated timber members are typically subjected to flexural forces and shear forces. Each of these force effects causes a different type of ultimate failure. Shear failures are brittle, sudden, and are usually more difficult to foresee. In structural design, the preferred mode of ultimate failure is flexural failure. This is because flexural failures are often ductile and slow. Significant amounts of cracking and distinct deflections indicate that flexural failure is approaching, but collapse may still be avoided. Little is known about the flexural behavior of NLT in industrial applications even though it is the favored type of failure in general timber design. The strength and stiffness of a nail-laminated assembly is dependent on several factors: the size, grade and species of lumber used; the number of laminations; the relative location of the butt joint(s) in each layer; and the type, amount and location of butt joint reinforcement, when used (Williams et al., 1994).

Current NLT design references are based on allowable stress design criteria specified for individual sawn lumber in the American Wood Council National Design Specification (NDS) for Wood Construction (2018) and include additional adjustment factors that account for the configuration of butt joints and the cross section. The NDS specifies that the reference bending design value for sawn lumber, F_b, multiplied by a series of adjustment factors, must be greater than or equal to the applied bending stress, f_b, at the section of the member in consideration. The reference bending design value is based on test results for specific species, commercial grades, and the size classification of the sawn lumber. The adjusted bending design value, F_b', specified in NDS Section 4.3, is computed using Equation 2.1 shown below. Definitions of variables used in all of the equations are shown in the Notation section of this thesis.

$$F_b' = F_b \times C_D C_M C_t C_L C_F C_{fu} C_i C_r \qquad 2.1$$

The applied bending stress, f_b, for solid wood members is specified in Equation 3.3-1 of the NDS and is shown in Equation 2.2. This equation applies to all wood members

subjected to flexure; the moment is dependent on the loading condition and the section modulus is dependent on the geometry of the cross section.

$$f_b = \frac{M}{S} \tag{2.2}$$

2.1.2 International Building Code (2018)

Nail-laminated timber has been accepted in the International Building Code (IBC) (2018) and utilized in various structural applications for buildings throughout the world. The 2018 IBC recognizes NLT in Section 2304.9.3 as "Mechanically Laminated Decking." Mechanically laminated decking is defined in Section 2304.9.3.1 of the 2018 IBC as square-edged dimensional lumber laminations set on edge and nailed to the adjacent pieces and to the supports. A typical cross section view of NLT is depicted in Figure 2.1. Although the IBC provides specifications for only building rather than industrial applications, the structural design recommendations are relevant to this research as NLT crane mats are typically subjected to similar loading. Specifically, the 2018 IBC details requirements for fastening laminations and end joint locations within individual layers. Though support connections are specified, only the design recommendations for the mechanically laminated decking pertained to this research.

Section 2304.9.3.2 of the 2018 IBC states that the length of nails connecting laminations shall be at least 2.5 times the net thickness of an individual lamination. The spacing between fasteners for lamination connections is based primarily on the support conditions. When mechanically laminated decking is supported across its entire width at 48 in. o.c. or more, nails should be installed perpendicular to the face of the lamination at a maximum distance of 18 in. o.c. When supports are located at less than 48 in. o.c., nails should be installed in the same fashion, but spaced at a maximum distance of 30 in. o.c. Crane mats are often supported along their entire length and they most closely relate to the second support condition. However, depending on the specific application, a crane mat may only be supported at its ends. The placement of nails should alternate between the top and bottom edges and be staggered within adjacent laminations as shown in Figure 2.2. The 2018 IBC specifies that nails penetrating through two laminations and partially into a

third be staggered at one-third of the spacing in the neighboring laminations. If nails penetrate entirely through three or more laminations, nails are only required to be staggered at one-half of the spacing in adjoining layers. Where butt-joints occur within individual laminations, two nails shall also be installed at each end of the jointed pieces. The maximum spacing for various nail sizes as specified by the 2018 IBC for mechanically laminated decking constructed with laminations having a nominal thickness of 2 in. is provided in Table 2.1.

A controlled random pattern of butt-joints is allowed by the 2018 IBC to construct mechanically laminated decking that spans greater distances than those that are achievable with standard lumber lengths. Section 2304.9.3.3 of the 2018 IBC specifies that there shall be a minimum distance of 24 in. between end joints in adjacent laminations. The first and second laminations are required to sit on at least two supports and the joints in these two laminations may only occur on alternate supports. After that, a maximum of seven intervening laminations are allowed to contain joints at random locations before the pattern specified for the first two laminations must be repeated.

The 2018 IBC specifies that the capacity of mechanically laminated lumber decking shall be determined in accordance with the 2018 NDS. Using allowable stress design, the flexural capacity and deflection can be calculated if the decking is constructed according to the previously described methods. The equations for the allowable area loads for flexure and deflection in Table 2306.1.4 of the 2018 IBC are shown in Equations 2.3 and 2.4, respectively.

$$\sigma_b = \frac{20F_b'd^2}{3l^2 6} \tag{2.3}$$

$$\sigma_\Delta = \frac{100\Delta E'd^3}{12l^4} \tag{2.4}$$

2.1.3 Nail-Laminated Timber U.S. Design and Construction Guide (2017)

Butt jointing laminations between supports is a common method of construction used to decrease the cost of NLT. However, constructing butt joints within the laminations results in a lower strength and stiffness that must be addressed in the design. In order to

account for cases where NLT laminations are butt-jointed between supports or NLT is constructed using laminations of varying depths, additional adjustment factors must be applied to the bending capacity shown in Equation 2.5 of this document.

The Nail-Laminated Timber U.S. Design & Construction Guide (NLT Design Guide, 2017) specifies that NLT should be designed for flexure using NDS provisions but requires that the NLT bending capacity, $F_{b.NLT}'$ is greater than the bending stress, f_b. The bending capacity is calculated by determining the individual lamination capacity according to NDS Section 4.3. The bending capacity is modified by additional adjustment factors to account for the layup and cross section type as described in Section 4.1.2 in the NLT Design Guide. The NLT adjustment factors were determined based on IBC Table 2306.1.4 and previous research (Haller, 2000; Kramer, 2003; Kramer, 2004). The modifications assume that the NLT behaves in a linear elastic manner per NDS Section 3.3, with the greatest stresses occurring at the extreme fiber of the section. The nail-laminated timber bending capacity, specified in NLT Design Guide Section 4.1.3, is computed using Equation 2.5.

$$F_{b.NLT}' = F_b' K_{layup.b} K_{section.b} \quad (2.5)$$

The adjustment factor for bending strength, $K_{layup.b}$, is based on four specific NLT layup types. The layup types are defined according to the support conditions and placement of butt joints. The adjustment factors for NLT bending capacity are specified in Table 4.1 of the NLT Design Guide and shown in Table 2.2. The NLT Design Guide specifies that when NLT is fabricated with laminations of varying depth, the fasteners do not provide adequate stiffness to ensure the system behaves in an entirely composite manner. In this case, it is not conservative to simply sum the bending capacity of the individual laminations. This is due to the deeper laminations reaching their maximum bending capacity prior to the laminations with shallower depths. The equation for the cross section adjustment factor for bending strength, $K_{section.b}$, is presented in Table 4.2 of the NLT Design Guide. However, the depth of the NLT was constant throughout the laminations for each specimen in this research. Therefore, a reduction in capacity due to the cross section was not applicable.

The bending stress equation for NLT, provided in the NLT Design Guide in Table 4.3, is shown in Equation 2.6. The maximum bending moment to be used in Equation 2.6 is specified in Table 4.1 of the NLT Design Guide and shown in Table 2.3.

$$f_b = \frac{6M}{b_{panel}d^2} \tag{2.6}$$

Deflection often controls the design of timber structures. The NLT Design Guide bases stiffness properties of NLT on NDS reference design values and prescribes additional adjustment factors to account for the layup type and cross section of the member. A simplified beam analogy is used to analyze NLT deflections and compare the results to Code and project standards. The stiffness, *EI*, is composed of the modulus of elasticity (MOE), *E*, and the moment of inertia, *I*, as specified in Section 4.1.4 of the NLT Design Guide. The equation to calculate stiffness in Section 4.1.4 of the NLT Design Guide is reproduced in Equation 2.7.

$$EI = E_{NLT}'I = E'K_{layup.E}K_{section.E}\frac{b_{panel}d^3}{12} \tag{2.7}$$

The adjustment factor for stiffness based on layup type, $K_{layup.E}$, that is used in Equation 2.7 is based on the four layup types specified in Table 4.1 of the NLT Design Guide and shown in Table 2.2. The equation for the cross section adjustment factor for stiffness, $K_{section.E}$, is shown in Table 4.2 of the NLT Design Guide. This equation is identical to the equation for the cross section adjustment factor for bending strength, $K_{section.b}$. Therefore, a reduction in stiffness due to the cross section was not applicable.

To determine the maximum possible live load deflection that NLT may experience, the NLT Design Guide provides formulas based on a combination of the lamination layup type and the support conditions. Table 4.1 in the NLT Design Guide lists the deflection equations, which are shown in Table 2.4. Additional deflection due to creep should also be considered in structural applications, but it was disregarded as long-term load testing was outside of the scope of this research.

The NLT Design Guide includes details and specifications for lamination fastening to ensure the vertical shear force is adequately transferred between laminations so they deflect equally. The recommended fastener patterns are based on nominal lamination widths of 2 in. and the use of 3 in. long nails with minimum diameters of 0.148 in. and 0.128 in. Nail locations are specified in either one row alternating along top and bottom edges or two rows. The specified patterns closely resemble the 2018 IBC and are categorized based on the nominal depth of the NLT member. Where butt joints are placed along laminations, two additional fasteners should be provided on each side of the joint. The fastener patterns are provided in Table 4.6 of the NLT Design guide and shown in Table 2.5.

2.2 Previous Research on NLT in Flexural Bending

2.2.1 Winistorfer, Moody, and Cramer (1987)

Winistorfer et al. (1987) investigated the bending performance of butt-jointed nail-laminated structural members by focusing on three variables: butt joint location, distance between butt joints, and presence of additional nail plates. A total of 32 nail-laminated posts were manufactured with three laminations and various configurations of joints. The specimens consisted of No. 2 hem-fir (a combination of western hemlock and true fir species) laminations with nominal dimensions of 2 x 6 in. and a length of 12 ft. The laminations were fastened together using 20-penny ring-shank nails. The nails were 4 in. long by 0.178 in. in diameter and placed in two rows at 12 in. o.c. on the wide face of the exterior laminations. Lengths of 2 and 4 ft between butt joints in the direction of the span were chosen and the locations were varied between midspan and 2 ft away from midspan of the specimens. An example of the 2 ft distance between butt joints, located at the middle of the specimen is shown in Figure 2.3. In addition to the butt-jointed specimens, a series of nail-laminated control specimens with continuous laminations were constructed and tested. The specimens were tested in accordance with ASTM D198 (ASTM, 1976) using a four point bending setup until flexural failure occurred. The four point bending test consisted of a support at each end of the specimen and two actuators, which applied uniform load across the entire width of the specimen.

Two general types of failures were observed during testing, which included lumber failure in tension and compression failure at the joint. The majority of the failures were

tension failures and cracking occurred at approximately 80% of the maximum applied point load. As a result of the testing, it became evident that the length between butt joints affected both the bending stiffness and strength of the member. A difference in the average ultimate load of 41% was observed when comparing specimens with 2 and 4 ft distances between butt joints, with the 4 ft spacing providing the greater capacity. However, whether the joints were located at midspan or offset from midspan had little effect on the ultimate strength. Despite the variety of NLT configurations, none of the butt-jointed specimens exhibited flexural performance equal to or greater than members with continuous laminations. In order to develop reliable design criteria, a much larger sample size would have been required. Instead, the study performed by Winistorfer et al. (1987) served as a pilot study that indicated what to expect from the results of a larger testing program.

2.2.2 Bohnhoff, Moody, Verrill, and Shirek (1991)

Bohnhoff et al. (1991) tested 140 NLT posts in bending to characterize the structural properties. The specimens were constructed of three laminations and had a total length of 12 ft. In addition to the 140 NLT specimens, 56 individual pieces of the lumber were loaded to failure in bending. The goal of Bohnhoff et. al. was to determine how bending strength and stiffness of single members of dimensional lumber, NLT with continuous laminations, and butt-jointed NLT (with and without joint reinforcement) compared to each other. The effect of fastener type and spacing on bending strength and stiffness of butt-jointed NLT was also investigated.

The NLT members were constructed of nominal 2 x 6 in. No. 1 dense southern pine lumber and fastened together using two different types of nails. The first fastener was a gun-driven 20d ring-shank nail with a length of 4 in. and a diameter of 0.145 in. and was used to construct half of the NLT specimens. The remainder of the specimens, including all of the butt-jointed members, were fastened together using a spirally threaded wire. The wire had a length of 4.5 in. and a diameter of 0.187 in. An autonailing machine was used to drive and cut the wires in a pattern of two rows at 18 in. o.c. The butt joints in the NLT specimens occurred in the first lamination at midspan and offset 2 ft in either direction for the adjacent layers, similar to Winistorfer et al. (1987).

The NLT specimens were subjected to a four point bending test with uniform loading according to ASTM D198 (ASTM, 1984). Specimens were loaded at a constant

rate of 0.40 in./min until flexural failure had occurred. The single pieces of southern pine lumber were tested in the same fashion to determine the modulus of rupture (MOR) and MOE for comparative analysis.

After testing, it was observed that the allowable bending stress for NLT members constructed of three continuous laminations was approximately 30% greater than the values corresponding to the single pieces of lumber. The average MOR of the NLT with continuous laminations was about the same as the single pieces of lumber, but the average MOR of the NLT specimens with continuous laminations had significantly lower variability. A comparison of the test results indicated that a reduction in strength was associated with the inclusion of butt joints. The maximum resulting bending strength for the butt-jointed members without any joint reinforcement were observed to be less than approximately 45% of the maximum bending strength values for the specimens with continuous laminations. Butt-jointed NLT specimens without any additional joint reinforcement averaged only 60% of the bending stiffness of that exhibited by the specimens with continuous laminations. When comparing the two types of fasteners used in this study, it was clear that there was no significant difference in the bending strength and stiffness of the NLT.

2.2.3 Williams, Bohnhoff, and Moody (1994)

The study conducted by Williams et al. (1994) was essentially an extension of the research performed by Bohnhoff et al. (1991) and had the same set of objectives. However, in this case, the NLT members were constructed of four laminations rather than three. The specimens were fabricated in a similar manner as the members with three laminations but differed in the distance between butt joints and overall specimen length. In this study, 20 ft long NLT specimens with distances between butt joints of 4 and 6 ft were investigated. Specimens were constructed of nominal 2 x 10 in. southern pine lumber and fastened together with gun-driven nails. The nails were 3.75 in. long and had a 0.130 in. diameter. They were placed in three rows at approximately 12 in. o.c. This same pattern was used for butt-jointed specimens, but the spacing was decreased to 3 in. within the field of the splice.

A total of 75 NLT specimens were tested using a four point bending test with a 19 ft simply supported span in accordance with ASTM D198 (ASTM, 1992). The load was applied as a rate of 0.50 in./min until the specimens failed in bending. Lateral supports

were placed along the length of the span to prevent any torsional effects that would be present in a standard four point bending test. Test results indicated that increasing the distance between butt joints from 4 to 6 ft provided an average increase in strength of 28% and the average stiffness increased by 5%. In conclusion, distance between butt joints and joint arrangement proved to affect the bending strength and stiffness of NLT members.

2.2.4 Haller (2000)

Nail-laminated timber is often idealized as lumber placed on center with a spacing equal to the width of one piece of lumber. However, when NLT is constructed with butt joints, the discontinuity in the laminations results in a decreased flexural capacity. Haller (2000) investigated the influence of the arrangement of butt joints on the structural behavior of NLT in an attempt to quantify the decreased capacity. Specifically, 12 NLT panels with an 8 ft long simply supported span with varying butt joint configurations were tested to determine the bending stiffness. The panels were constructed of kiln-dried spruce boards and were fastened together using an automatic nailing machine. A four point bending test with uniform and additional point loading in the transverse direction was conducted in an attempt to understand the effects of irregular butt joint placement on NLT bending stiffness. To prevent increased deflections due to creep, specimens were loaded and unloaded until a constant deformation was achieved and the specimen fractured.

The NLT test results suggested that the configuration and stiffness of the butt joints impacted the structural behavior of the panels. Where butt joints were placed in a straight line through every other lamination, the bending stiffness was approximately 20% less than panels constructed with continuous laminations. The NLT panels with butt joints distributed randomly behaved approximately 20% better than those with butt joints in a straight line through every other lamination. The resulting distribution of maximum strength and stiffness was low because the specimens were fabricated with many laminations, which created a more homogeneous structural element. It was concluded that the configuration of joints affects the flexural performance, although construction costs may be reduced by butt-jointing laminations.

2.2.5 Finite Element Modeling of NLT

In recent years, the majority of studies have used finite element modeling (FEM) rather than experimental testing to determine the behavior of butt-jointed NLT. Finite

element modeling was used to simulate NLT with numerous material properties, butt joint locations, and fastening methods. Realistic stiffness and strength values of individual pieces of lumber and the realistic load deformation characteristics of nailed timber were used in previous FEM studies. Haller (2000) simulated NLT subjected to four point bending and compared the results to experimental test results described in Section 2.2.4 of this document. The FEM results indicated that the modeling technique was validated and corelated with the experimental results of butt-jointed NLT where bending capacity was approximately 80% of the capacity of NLT with continuous laminations. Kraemer (2004) also simulated a variety of NLT designs and compared the results to physical test results obtained by Kraemer and Blass (2001). In this case, a three point bending test was modeled. The three point static bending test was similar to the four point bending test used in previous research, but only a single load was applied rather than two loads. Each NLT design was simulated 100 times and the bending stiffness of the models showed good agreement with the results of physical testing performed by Kraemer and Blass (2001). Finite element modeling has been accepted by the NLT Design Guide (2017) for use in determining adjustment factors for flexural behavior of NLT with layups that are not prescribed in current design recommendations. However, FEM designs should still be verified through experimental testing (NLT Design Guide, 2017).

2.3 Literature Review Summary

This chapter has summarized the current NLT flexural design standards as well as the previous research related to the bending performance of NLT with butt-jointed laminations. Nail-laminated timber has been included in building codes for over a century, however, most design resources are dated and focus on prescriptive rather than engineered applications. As a result, little research has been conducted to understand the flexural behavior of NLT with numerous butt joints. Additionally, there is an absence of literature that examines NLT constructed with rough cut lumber instead of dimensional lumber.

Nail-laminated timber is currently going through a resurgence and, while it has been implemented in building applications, industrial use is not yet widespread. Crane mat design with NLT is advantageous because it offers an economically available alternative to products currently used in industry (e.g., composite, steel framed, solid timber, CLT).

Although there is a variety of crane mat systems in existence, the majority of designs are proprietary and there is no body governing or standardizing the design and performance.

The literature indicated that the inclusion of butt joints within laminations of NLT reduced the flexural capacity compared to NLT constructed with continuous laminations by approximately 20 to 60%. Furthermore, the literature suggested that the flexural capacity continued to decrease as joints were placed closer together in both the direction of the span and adjacent laminations. The design standards for flexural strength of NLT are recognized as adequate for structural applications, but when materials and construction methods deviate from current specifications, it is important that they be compared to experimental or FEM test results (NLT Design Guide, 2017). Ultimately, the variability between NLT designs requires extensive testing to quantify the bending performance.

Table 2.1. Nail size and spacing as specified in the 2018 IBC

Minimum Nail Size (Length x Diameter) (in.)	**Maximum Spacing Between Nails (in.)**	
	Decking Supports Spaced ≤ 48 in.	**Decking Supports Spaced > 48 in.**
4 x 0.192	30	18
4 x 0.162	24	14
4 x 0.148	22	13
3.5 x 0.162	20	12
1.5 x 0.148	19	11
3.5 x 0.135	17	10
3 x 0.148	11	7
3 x 0.128	9	5
2.75 x 0.148	10	6
2.75 x 0.131	9	6
2.75 x 0.120	8	5

Table 2.2. NLT bending capacity adjustment factors for layup types as specified in the NLT Design Guide (2017)

Layup Type	**Adjustment Factor**	
	Bending Strength ($K_{layup.b}$)	**Stiffness ($K_{layup.E}$)**
Laminations continuous and single span	1.0	1.0
Laminations continuous and multi-span	1.0	1.0
Laminations with controlled random butt joints over four or more supports	0.67	0.69
Laminations with controlled random butt joints over fewer than four supports	$0.202\frac{(l/d)^{1/4}}{s^{1/9}}$	$0.0436\frac{(l/d)^{9/10}}{s^{1/5}}$

Table 2.3. Maximum bending moments for layup types as specified in the NLT Design Guide (2017)

Layup Type	**Maximum Bending Moment**
Laminations continuous and single span	$M = \frac{wl^2}{8}$
Laminations continuous and multi-span	$M = \frac{wl^2}{8}$
Laminations with controlled random butt joints over four or more supports	$M = \frac{wl^2}{10}$
Laminations with controlled random butt joints over fewer than four supports	$M = \frac{wl^2}{8}$

Table 2.4. Maximum live load deflection equations for layup types as specified in the NLT Design Guide (2017)

Layup Type	**Maximum Deflection (Δ)**	
Laminations continuous and single span	$\frac{5wl^4}{384E(d^3/12)}$	
Laminations continuous and multi-span	$\frac{wl^4}{185E(d^3/12)}$	
Laminations with controlled random butt joints over four or more supports	$\frac{wl^4}{145E(d^3/12)}$	
Laminations with controlled random butt joints over fewer than four supports	single span: $\frac{5wl^4}{384E(d^3/12)}$	double span: $\frac{wl^4}{185E(d^3/12)}$

Table 2.5. Lamination fastener patterns as specified in the NLT Design Guide (2017)

NLT Type	**NLT Nominal Depth**	**Nailing Pattern**	
		3 in. long, 0.148 in. diameter nails (staggered)	**3 in. long, 0.128 in. diameter nails (staggered)**
Continuous Laminations	Less than 6 in.	One row @ 7 in. o.c.	One row @ 5 in. o.c.
	More than 6 in.	Two rows @ 14 in. o.c.	Two rows @ 10 in. o.c.
Butt-Jointed Laminations	Less than 6 in.	One row @ 7 in. o.c.	One row @ 5 in. o.c.
	More than 6 in.	Two rows @ 10 in. o.c.	Two rows @ 10 in. o.c.

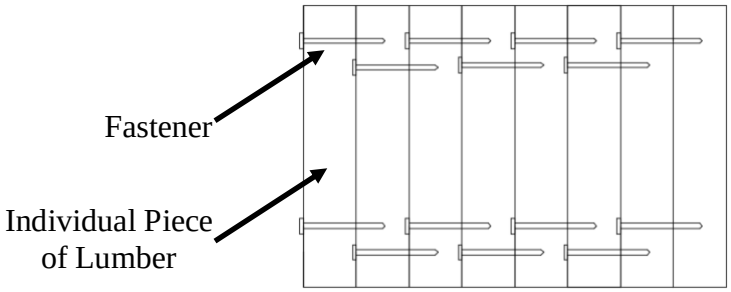

Figure 2.1. Typical NLT cross section

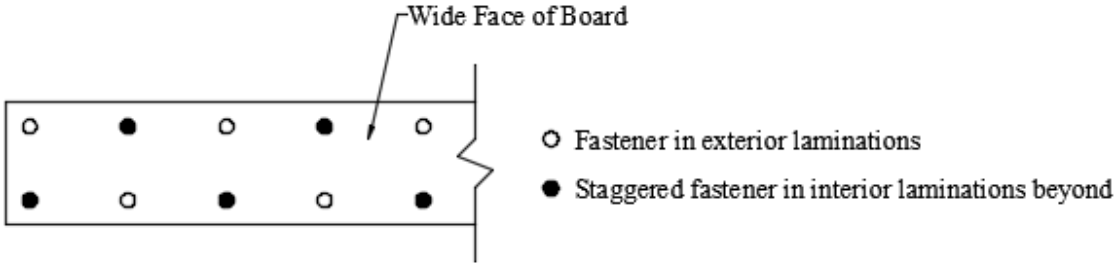

Figure 2.2. One row of fasteners staggered between the top and bottom of the wide face as specified in the 2018 IBC

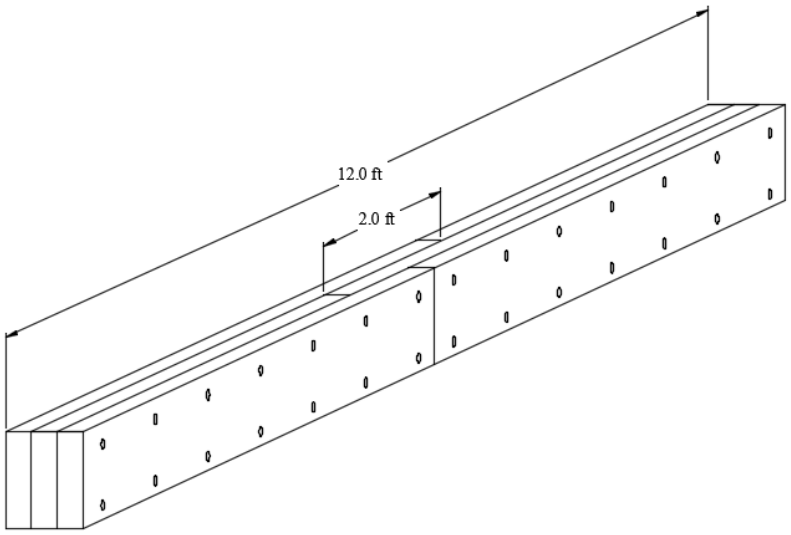

Figure 2.3. Distance of 2 ft between butt joints investigated by Winistorfer et al. (1987)

CHAPTER 3. LABORATORY SPECIMEN DESIGN AND TEST METHODS

3.1 Mat Design and Fabrication

This section provides details on the nail-laminated timber mat design, fastener types, fastener patterns, and nail-laminated timber mat fabrication. Six NLT beams, approximately 7 in. wide x 8 in. deep x 16 ft long, were fabricated at Savanna Pallets, Inc. and transported to the University of Minnesota Duluth (UMD) structures laboratory along with two 7.5 in. wide x 7.5 in. deep x 16 ft long solid timber beams. Two more 7 in. x 8 in. x 16 ft NLT beams and a 4 ft wide x 8 in. deep x 16 ft long NLT mat were fabricated at the UMD structures laboratory.

3.1.1 Mat Design Materials

3.1.1.1 Lumber

Northern red oak was selected as the species of lumber to be used in all test specimens. This particular species was chosen because it was locally accessible and currently underutilized in the northern Minnesota region. The local accessibility ensured that there would be a sustainable supply for full scale manufacturing. Typically, lumber is cut and dressed to consistently produce a specific size, but for this research the lumber was left rough cut. Being a low-grade lumber, the northern red oak boards contained several knots and exhibited visible moisture at various locations as shown in Figure 3.1. The lumber was dried at Savanna Pallets, Inc. for use in four of the test specimens, while the remaining lumber was left in its natural, moist state, commonly referred to as green. Physical and mechanical properties of lumber used in structural applications are commonly determined through a series of rigorous American Society for Testing and Materials (ASTM) testing, however, the properties of the lumber used in this research were unknown. To accommodate the manufacturing capabilities of Savanna Pallets, Inc., boards were cut to a thickness of approximately 1.25 in. and a width of roughly 7 in. Due to the direct relationship between cost and increasing board length, the lumber used in this research was limited to a maximum length of 8 ft. A series of tests were performed at the NRRI in accordance with ASTM D143 (ASTM, 2014) to determine the MOE and average moisture content of the lumber.

3.1.1.2 Fasteners

Three types of fasteners were chosen to connect the individual laminations together into a solid structural member. The first fastener was a #12 x 5-5/8" R4^{TM} Multi-Purpose Framing Screw manufactured by GRK Fasteners. The screw was a dowel-type, multipurpose screw used in wood-to-wood connection applications. The screw was 5.5 in. long and had a 0.17 in. diameter at the shank. The screw was made of case hardened steel and covered in a proprietary coating for corrosion resistance. The International Code Council (ICC) Evaluation Service's ESR-3201 Evaluation Report (2017) verified that the R4^{TM} Multi-Purpose Framing Screw was in compliance with the 2015 IBC and approved for structural applications.

The second fastener was a 20° Plastic Strip Jumbo Scrail manufactured by Beck Fastener Group. Scrails are similar to common screws in that they are threaded along a portion of their shank. However, they differ in the method of installation. Screws are driven into the material with a drill, but scrails are inserted using a pneumatic nail gun. The scrails used in this research had a length of 4 in. and a shank diameter of 0.148 in. The 20° Plastic Strip Jumbo Scrail was made of common steel and electrogalvanized for corrosion resistance. Common scrail applications include, but are not limited to, framing, decking, and sheathing (Beck, 2018).

The third fastener was a 15° Wire Coil Nail manufactured by Hammerstrike Fasteners. The nail was 3 in. long and had a 0.120 in. diameter at the shank. The nails were made of steel and covered in a zinc coating. Wire-collated nails are typically used for pallet construction and wall framing and are best suited for high volume worksites (Koen, 2018). The 15° Wire Coil Nails were installed using a pneumatic coil nailer. Figure 3.2 displays the R4^{TM} Multi-Purpose Framing Screw, Wire Coil Nail, and the Plastic Strip Jumbo Scrail used in the construction of the NLT specimens.

A second form of fastening was required for the full size NLT mat specimen to behave compositely during testing. Four threaded stainless steel rods, manufactured by The Hillman Group, were used in conjunction with washers and nuts to bolt the full size NLT mat together. The steel rods had a 0.375 in. shank diameter and were finished with a zinc plating. The washers were 0.5 in. diameter stainless steel fender washers. The nuts were 0.375 in. diameter hex nuts, made of stainless steel and plated with zinc. The mechanical

properties were not measured or obtained from the manufacturer as the bolting mechanism was intended to bind the NLT rather than add flexural strength.

3.1.2 Laboratory Specimen Types and Sizes

Eleven specimens were tested in the laboratory to evaluate the flexural strength of NLT crane mats constructed with the materials chosen for fabrication. The mat specifications were atypical of NLT designed in accordance with the IBC (2018) and NLT Design Guide (2017) because the primary objective of this research was to assess the flexural strength characteristics of NLT mats fabricated with low value lumber and non-traditional fasteners. The test specimens were predominantly designed to determine a final product that could be mass produced by Savanna Pallets, Inc. In order to quantitatively predict the flexural performance of each specimen prior to testing, a statistically significant dataset of lumber properties would be required. Fastener properties, fastener patterns, and joint locations would have to align with code specifications to produce reliable calculations. Instead, this research aimed to assess the performance of the provided materials and compare the experimental capacities to theoretical capacities of NLT constructed using low grade rough cut lumber with known material properties.

The specimens tested included a total of eight NLT beams, one full size NLT mat, and two solid timber beams. The two solid timber beams were tested first to provide a baseline of flexural performance for comparison to all of the testing results from the testing matrix. Of the eight NLT beams, four of the specimens built with lumber were dried at Savanna Pallets, Inc. prior to being shipped to UMD. Two of these dried specimens were fastened together with screws placed in one row alternating between the top and bottom at 10 in. o.c., while the other two were fastened together with nails placed in two rows at 7 in. o.c. The remaining four NLT beams were left green to evaluate the effect of moisture content on the flexural performance. The moisture content of the dried specimens was unknown, but the moisture content of the green lumber was determined from ASTM test results. One of the green specimens was fastened together with screws, one with nails, and the remaining two with scrails. The full size NLT mat was constructed of an additional six, green NLT beams, which had approximately the same dimensions as the previously described specimens. The six NLT beams were bolted together with threaded steel rods through the wide face of the lumber to represent a final product similar to crane mats

currently used in the local industry. A summary of the type and size of specimen tested in the laboratory, including exact dimensions, can be found in Table 3.1.

3.1.3 Mat Design

The NLT specimens were designed in three distinct phases. The preliminary phase consisted of determining initial design options for laminated timber mats, including dimensions of timbers, orientation of timbers, and fastening methods. The second phase included developing a set of preliminary specimens and testing them to determine their flexural strength characteristics. The final phase entailed revising the preliminary design by prescribing joint locations and implementing a less common fastener to connect the individual laminations. Savanna Pallets, Inc. governed the test specimen design decisions with the goal of producing a final crane mat design that would be comparable in look and performance to those used in the local industry.

The first phase of design began with Savanna pallets selecting a CLT mat design. The design consisted of five layers of lumber placed on their wide face, often referred to as the weak axis, with each layer oriented perpendicular to the adjacent layers. The lumber in the top and bottom layers spanned across the width of the mat rather than the length, which was opposite of common CLT designs. This option was quickly omitted after a prototype was tested in the field by United Piping, Inc. and immediately exhibited poor performance. The orientation of lumber in the top and bottom layers provided less strength compared to an orientation of lumber placed parallel to the length of the mat. Furthermore, as heavy equipment drove onto the mat, the individual boards split and revealed steel fasteners, which posed a threat of puncturing tires on equipment and vehicles. Two of the field tested CLT mats with broken edges and protruding fasteners are shown in Figure 3.3. A design using adhesives to laminate the individual layers was also proposed, but this option was abandoned due to the high moisture content of the lumber being used, which prevented proper adhesion at ambient temperatures. Finally, a NLT method of design was chosen as it could easily be manufactured and utilize the strong axis (direction parallel to the grain) of the lumber, while preventing fastener protrusion on the driving surface. Once the design methodology was determined, materials were chosen for fabrication of the NLT specimens. Savanna Pallets, Inc. and the NRRI selected all design materials based on cost and availability. A series of tests were performed at the NRRI on 1 in. wide x 1 in. deep x

16 in. long pieces of lumber to determine the unknown material properties that were required for this research.

The second phase of design consisted of constructing and testing a preliminary set of NLT specimens. Six 16 ft long NLT specimens were fabricated using six laminations of northern red oak lumber. Butt joints were randomly placed along the individual laminations at 2, 4, 6, and 8 ft. Figure 3.4 through 3.9 show plan views that detail the joint locations of the preliminary NLT specimens listed in Table 3.1. The location of each joint was chosen by Savanna Pallets, Inc. Rather than constructing a series of mats of standard width (approximately 4 ft), the specimens resembled built-up beams having only six laminations (approximately 7 in. wide). This design was chosen to avoid unnecessary costs, while still creating a specimen that was representative of a full width NLT mat. The preliminary NLT specimens were then transported to the UMD Structures Laboratory and tested along with two solid timber beams. A solid timber beam specimen is shown in Figure 3.10.

The third phase of design began with an evaluation of the preliminary NLT specimens. After testing, each type of lamination layup and fastener type was assessed based on its performance. To avoid any eccentric loading during testing, the layup of laminations was revised so joint locations were oriented to produce a symmetric layup in plan view, as shown in Figure 3.11. The NRRI recommended implementing steel scrail fasteners in this design phase. Two more 16 ft long NLT beams, each made of six laminations, were fabricated using a symmetric layup and scrails and tested at the UMD structures laboratory. In addition to the two NLT beam specimens, six more specimens of the same design were constructed and bolted together to form the 4 ft wide NLT mat, which was tested in the same fashion.

3.1.4 Specimen Fabrication

The NLT specimens tested in this research were constructed using a fairly simple fabrication process. The three NLT beams fastened together with R4^{TM} Multi-Purpose Framing Screws were each constructed by first stacking six laminations (approximately 8 in. x 1.25 in. x 16 ft) of the northern red oak lumber flat on the floor. The weight of the lumber was sufficient to keep the laminations in place while they were fastened together. Screws were drilled vertically into the lumber from the exterior wide face of the top lamination using a cordless power drill. The screws were placed in one row, alternating

between the top and bottom at approximately 10 in. o.c. throughout the length of each NLT beam. The specimens were then carefully flipped over to the other exterior lamination and screws were installed using the same pattern. The screws penetrated entirely through three laminations and partially into the fourth. For the preliminary specimens, butt joints were placed randomly throughout laminations to make 16 ft long specimens. However, joints occurring in the same location in more than one lamination were separated by two intervening laminations. Figure 3.12 displays the pattern of the R4^{TM} Multi-Purpose Framing Screws.

The three specimens that were fastened together using the 15° Wire Coil Nails were constructed by first stacking three laminations of the lumber with the wide face flat on the floor. The nails were inserted vertically into the exterior wide face of the top lamination using a pneumatic nail gun. The nails were placed in two rows at approximately 7 in. o.c. along the length of the specimen. The three connected laminations were flipped over and nailed in the same manner, but slightly offset so the nails would not hit those placed in previous laminations. Next, an additional lamination was placed on top and nailed to the initial three layers using the same pattern of two rows spaced at 7 in. o.c. This process was repeated until a total of six laminations were fastened together.

The three remaining NLT specimens were fabricated at the UMD structures laboratory using equipment provided by Savanna Pallets, Inc. Two NLT beams were constructed by first stacking four laminations of the lumber with the wide face flat on the floor. The laminations were fastened together with 20° Plastic Strip Jumbo Scrails using a pneumatic strip nailer. Scrails were placed in two rows at 20 in. o.c. The NLT beams were flipped and scrails were placed in the same fashion along the length of the exterior lamination, but slightly offset to ensure the scrails would not collide. Next, an additional lamination of lumber was stacked on top and fastened to the other four layers with scrails placed in two rows at 10 in. o.c. Finally, the specimen was flipped back over and a sixth lamination was added by fastening it to the adjacent layers using two rows of scrails located at 10 in. o.c. Butt joints in the specimens fastened together with scrails were located to provide a symmetric layup of laminations, as shown in Figure 3.11. An elevation view depicting the scrail fastening pattern can be seen in Figure 3.13. All fastening in exterior

laminations was in accordance with the 2018 IBC, but fastener spacing was not reduced in neighboring laminations as described in section 2.1.2 of this document.

The six NLT beams used to construct the full size NLT mat were fabricated at the UMD structures laboratory in the same fashion as the three specimens fastened with scrails. The NLT beams were placed on edge and four 1/2 in. diameter holes were drilled at 5 ft o.c., with the first hole located 6 in. from the end of the specimens. The NLT beams were clamped together and threaded stainless steel rods were inserted through the entire width (all six NLT beams). Finally, the washers and nuts were placed on the ends of the threaded rods and the clamps were released to produce the final product. The full size NLT mat being moved into the test setup is shown in Figure 3.14.

3.2 Testing Setup, Instrumentation, and Procedure

3.2.1 UMD Flexural Strength Test Setup

All of the tests were performed using a simply supported span and a single, transverse point load as specified in ASTM D198 (ASTM, 2015). In addition to ASTM standards, the American National Standards Institute (ANSI)/APA – The Wood Association PRG 320 Standard for Performance Rated CLT (PRG 320, 2012) was used to select the test setup. PRG 320 is intended for the testing of CLT, but was used to determine the span length for NLT testing as it was not specified in ASTM D198 (ASTM, 2015). A span length of approximately 30 times the specimen depth was recommended by PRG 320 (PRG 320, 2012), but a span of roughly 22.5 times the depth was chosen for testing. Although crane mats are often continuously supported on the ground in the field, the test setup used in this research was chosen to represent the worst-case loading scenario and provide basic information pertaining to the bending characteristics of butt-jointed NLT mats. The 16 ft long specimens were supported with a span of 15 ft, and a 6 in. overhang remained beyond the center line of each support. A single actuator, attached to the steel load frame, was placed at the center of the 15 ft span. An even distribution of load across the section at the location of loading and the support was crucial to guarantee each specimen behaved as a composite member when loaded. Only a portion of the laminations would have been engaged if loading or support conditions did not allow for a uniform distribution of the load. To ensure the load was distributed equally across the section, the surface of the specimens at the location of the load and each support was leveled using a

handheld belt sander. Loading conditions and pin-and-roller support conditions were chosen to ensure a fully composite system with all laminations of the member reaching their maximum bending capacity.

To attain the simply supported, pin-and-roller support conditions, a solid 4 in. diameter steel cylinder that extended beyond the full width of each specimen was used to support each end of the member. Due to the limited area of the steel cylinder in contact with each specimen, a steel reaction bearing plate was used between the specimens and the cylinders to uniformly distribute the load. These steel plates were 6 in. wide and 48 in. long, which provided support across the entire width of each specimen as required by ASTM D198 (ASTM, 2015). The pin-and-roller arrangement was secured atop built-up, steel W-shape beams, as shown in Figure 3.15. To address any instability in the supports, HSS straps were placed over the W-shape beams and bolted to the concrete reaction floor.

Force was applied using a hydraulic actuator, which contacted the specimens as a single point load at the center of the span. The load was transmitted from the actuator to each specimen transversely through a steel spreader beam and additional HSS beam. Specifically, a 4 ft long W8x31 stiffened steel spreader beam was attached to the actuator crosshead. A 4 ft long HSS5x5x3/8 section was secured beneath the spreader beam to allow for adequate vertical displacement of the actuator during testing. The hydraulic actuator was mounted to a steel load frame, which was bolted to the reaction floor to establish a rigid, closed loading system as required by ASTM D198 (ASTM, 2015). The test setup, with the full size NLT specimen in position for testing, can be seen in Figure 3.16.

3.2.2 UMD Testing Instrumentation and Data Acquisition

A load cell and a linear position transducer (string pot) were used to record the applied load and corresponding deflection of each specimen throughout testing, respectively. To visually compare deflection and failure characteristics between specimens, a video camera was placed on each side of the load frame at the middle of the span. One camera was arranged to provide an overall view of the test area and the other camera was positioned next to the location of loading.

The load cell was an Interface Model 1000 Fatigue Rated Load Cell and possessed a capacity of 100 kips. The load cell was calibrated prior to the testing of all specimens. The load cell was positioned directly underneath the actuator at midspan. The measured

force was transmitted from the load cell to the data collection system as a voltage and converted to the applied load.

Deflection was measured using the string pot. The string pot was a UniMeasure P510 Series transducer with a direct current voltage output ranging from -5 to +5 volts. The string pot measured deflection to an accuracy of 0.01 in. and allowed for a stroke of approximately 15 in. In order to take measurements, the string pot was fixed to a steel base at the center of the 15 ft span, beneath the applied load, and encased by a cover made of steel and timber to prevent any damage caused by the deflecting mats. The end of the wire cable that exited the top of the string pot was attached to each specimen at approximately mid-depth by inserting a screw approximately 2 in. into the side of the specimen and clipping the wire to the head of the screw. The string pot was adjusted so the zero voltage output was positioned at the center of the stroke and the output range spanned the full length of the stroke. The string pot was calibrated prior to testing and it was verified that the relationship between displacement and voltage was linear across the full stroke of the wire cable. A linear variable differential transformer within the actuator was also available to measure displacement but was not used as ASTM D198 (ASTM, 2015) required an external means of measuring displacement. Figure 3.16 displays an elevation view of the test setup with the instrumentation. A step-by-step guide to install and set up the string pot is presented in Appendix A.

Data from each test were collected using a Shore Western control system and a National Instruments data acquisition system. Data were recorded at a rate of 10 samples per second (10 Hz) for both load and displacement. The load cell and string pot were calibrated within this system before testing began. To properly amplify the string pot output voltage to span the full scale of travel, the jumper configuration was set to unity gain. This was done by adjusting the first-stage and second-stage gain jumper positions according to the model of string pot used in the test setup. The gathered data were transcribed as text files and later reproduced as Microsoft Excel files to be used for further analysis.

3.2.3 UMD Flexural Strength Test Procedure

The focus of the testing on each specimen at UMD was to collect data pertaining to the flexural performance of the NLT crane mats. Before testing began, preparation and documentation of each specimen was required. The specimen was arranged under the load

frame and instrumented with the string pot. Prior to testing, photographs were taken of each specimen to document the test setup and any variation among specimens (e.g., joint locations, fastener locations, knots, and defects). The actuator was then moved into place and lowered to just above the surface of the specimen. Finally, the string pot and load cell were tared (zeroed).

Once test preparation was complete, the specimen was loaded at a constant deformation rate of 0.012 in./sec until ultimate failure. The load rate was chosen to allow for a test length of at least 4 minutes, as specified in ASTM D198 (ASTM, 2015). The average length of each test was approximately 15 minutes. After ultimate failure had occurred, the load was released from the specimen and the specimen was photographed to document the type and manner of failure. The specimen was removed from the test setup and stored in the UMD structures laboratory for examination and reference until analysis of the data were completed.

This test setup was successful in providing reliable data, but it experienced a minor problem due to pinned connections at both the top and bottom of the actuator. When the actuator was positioned above the specimen with any eccentricity, the load would become unbalanced and the actuator would push away from the specimen. This warranted a retest of the specimen as ultimate failure had not yet occurred. To avoid this issue during subsequent tests, the actuator position was ensured to be perpendicular to the specimen, and the location was precisely verified using torpedo levels.

3.2.4 NRRI MOE Test Setup

In addition to the NLT testing done at UMD, testing was performed at the NRRI to measure the stiffness of the northern red oak lumber. Specifically, 20 specimens cut from the northern red oak were subjected to a three point static bending test in accordance with ASTM D143 (ASTM, 2014) to characterize the MOE of the species. The 16 in. long x 1 in. wide x 1 in. deep specimens were prepared by Savanna Pallets, Inc. using a thickness planer, table saw, and miter saw. The test setup consisted of a 14 in. span with the single point load applied using a rigid wooden bearing block with a radius of 1.5 in. The bearing block was attached to the hydraulic actuator and mounted to the Instron 5585H load frame. The specimens were supported at each end using bearing plates and rollers to allow for both rotation and translation. The bearing plates and rollers were also adjustable laterally

in case the specimens were subjected to torsion. The supports were attached to a 4 ft steel support beam, which was fixed to the load frame. The wooden bearing block and support conditions for the MOE test setup at the NRRI are shown in Figure 3.17.

3.2.5 NRRI Testing Instrumentation and Data Acquisition

Load and midspan deflection data were recorded during testing to compare the MOE and of the twenty specimens to the MOE of the NLT specimens that were tested at UMD. To measure the applied load and vertical deflection at midspan, a load cell and deflectometer were implemented in the test setup. The deflectometer was a single arm Epsilon 3540-200T-ST Deflectometer with an attached spherical contact tip. The base of the deflectometer was mounted to the 4 ft steel support beam and the arm extended to the midspan of each specimen as seen in Figure 3.18. The arm of the deflectometer was spring loaded and had a stroke of 3 in. A steel thumb screw was placed at mid-depth of each specimen at the center of the simple span, and the contact tip of the deflectometer was positioned directly underneath the screw. The load cell used for data collection was an Instron 5585H Load Cell with a capacity of 52.6 kips.

Bluehill Materials Testing Software installed on the Instron computer at the NRRI was used for data acquisition during testing. Data were collected at a constant rate of 10 samples/sec (10 Hz). Both the load cell and deflectometer were calibrated within the software before the start of testing. The data from the Bluehill Materials Testing Software were converted into Microsoft Excel files for examination after testing was complete.

3.2.6 NRRI MOE Test Procedure

The length, width, depth, and mass of the specimens were measured using a caliper and laboratory scale prior to testing. Each specimen was marked at mid-length with a line to help position the specimen within the test setup. Table 3.2 displays the exact dimensions of the 20 specimens tested at the NRRI to determine the MOE. Each specimen was centered on the supports with the long axis oriented perpendicular to the load point and supports. Once the specimen was in place, the wooden loading block was lowered close to, but not in contact with, the specimen. Subsequently, the load was applied at a rate of 0.05 in./min as specified in ASTM D143 (ASTM, 2014) until the maximum applied point load was achieved. Photographs were taken of each specimen before and after testing to identify the failure mode.

After specimen failure, a block that was approximately 1 in. long was cut from five specimens near the point of failure. The blocks were used to determine the initial moisture content of the northern red oak species in accordance with ASTM D143 (ASTM, 2014). The five block subsamples were then weighed and the mass was recorded. After that, the subsamples were placed into a pre-warmed oven set at a temperature of 217°F for approximately 24 hours. Finally, the subsamples were removed from the oven, reweighed, and the mass was recorded again to determine the average moisture content.

Table 3.1. Type and size of specimen tested in the laboratory

Specimen Type	Width (in.)	Depth (in.)	Length (in.)
Solid Timber (1)	7.375	7.25	197.875
Solid Timber (2)	7.5	7.5	195.5
Dried, Nailed NLT (1)	8.0	7.0	192.0
Dried, Nailed NLT (2)	8.0	7.125	191.975
Dried, Screwed NLT (1)	7.875	7.125	191.75
Dried, Screwed NLT (2)	8.125	7.25	192.0
Green, Nailed NLT	7.125	7.5	191.75
Green, Screwed NLT	7.625	6.875	192.0
Green, Scrailed NLT (1)	6.875	7.625	193.0
Green, Scrailed NLT (2)	7.0	7.875	192.5
Green, Scrailed NLT Mat	41.5	7.625	193.25

Table 3.2. Dimensions of the specimens tested at the NRRI to obtain MOE

Specimen	Width (in.)	Depth (in.)	Length (in.)
1	1.0135	1.0255	15.9695
2	1.0175	1.0195	15.8280
3	1.0130	1.0005	15.9980
4	1.0210	1.0175	15.9550
5	1.0225	0.9705	15.9665
6	1.0345	1.0195	16.0260
7	1.0285	1.0070	15.9615
8	1.0215	1.0115	15.8800
9	0.9850	1.0030	15.9460
10	1.0290	1.0220	16.0250
11	1.0405	1.0275	15.9760
12	1.0205	1.0160	15.9930
13	1.0260	1.0240	15.9705
14	1.0175	1.0275	15.9735
15	1.0050	1.0095	15.8235
16	1.0190	1.0205	15.9900
17	1.0145	1.0235	16.0060
18	1.0155	1.0075	15.8560
19	1.0130	0.9740	15.9850
20	1.0285	1.0290	15.9905

Figure 3.1. Northern red oak lumber with knots and visible moisture

Figure 3.2. Screw, scrail, and nail fasteners used for construction of the NLT specimens

Figure 3.3. Two stacked field tested CLT mats that were broken at the edges and revealed sharp steel fasteners

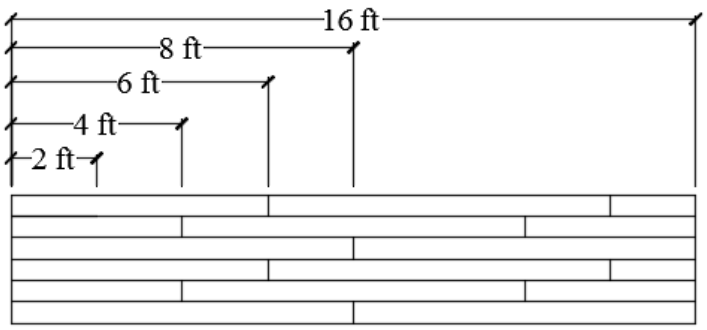

Figure 3.4. Plan view of Dried, Nailed NLT (1) showing butt joint locations in each layup with vertical lines

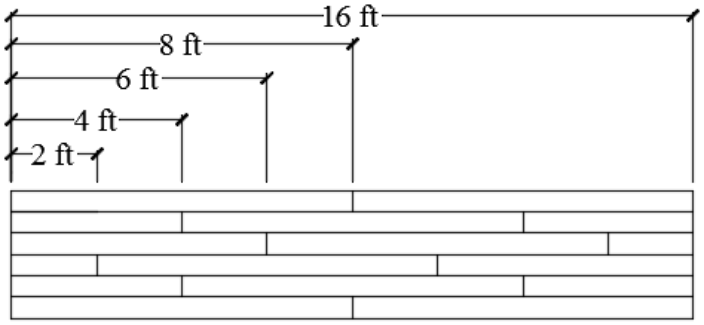

Figure 3.5. Plan view of Dried, Screwed NLT (1) showing butt joint locations in each layup with vertical lines

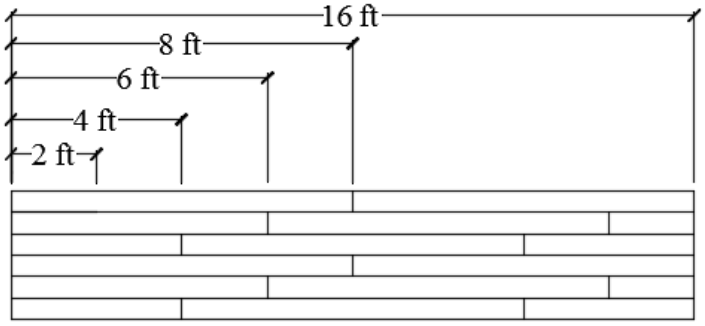

Figure 3.6. Plan view of Dried, Nailed NLT (2) showing butt joint locations in each layup with vertical lines

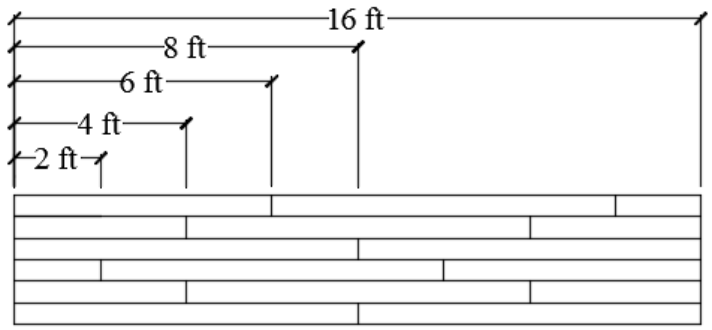

Figure 3.7. Plan view of Dried, Screwed NLT (2) showing butt joint locations in each layup with vertical lines

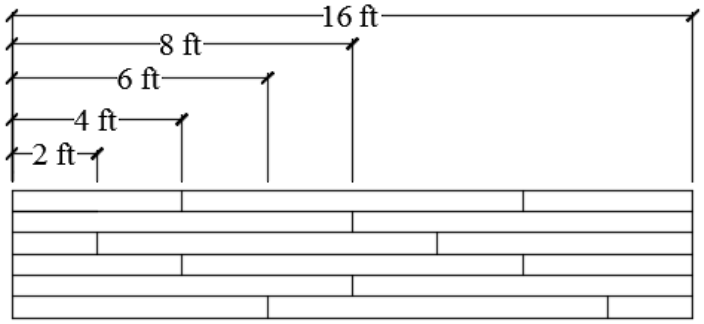

Figure 3.8. Plan view of Green, Nailed NLT showing butt joint locations in each layup with vertical lines

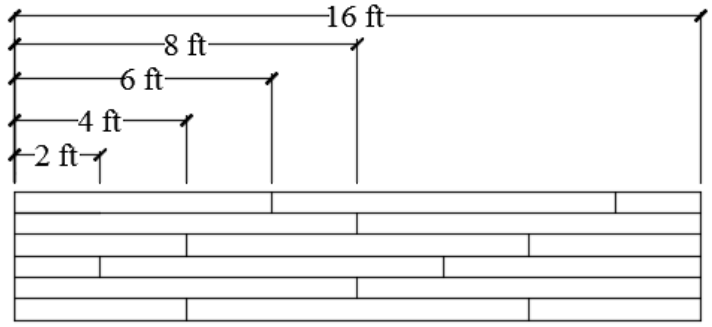

Figure 3.9. Plan view of Green, Screwed NLT showing butt joint locations in each layup with vertical lines

Figure 3.10. Solid timber beam placed in the test setup

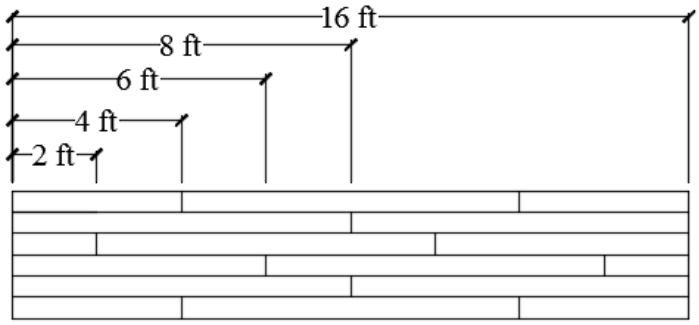

Figure 3.11. Plan view of symmetric lamination layup showing butt joint locations in each layup with vertical lines

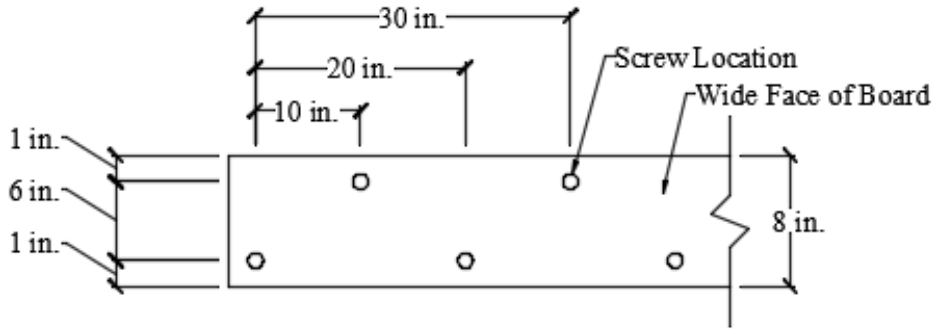

Figure 3.12. Elevation view of the fastener pattern for the R4^{TM} Multi-Purpose Framing Screw

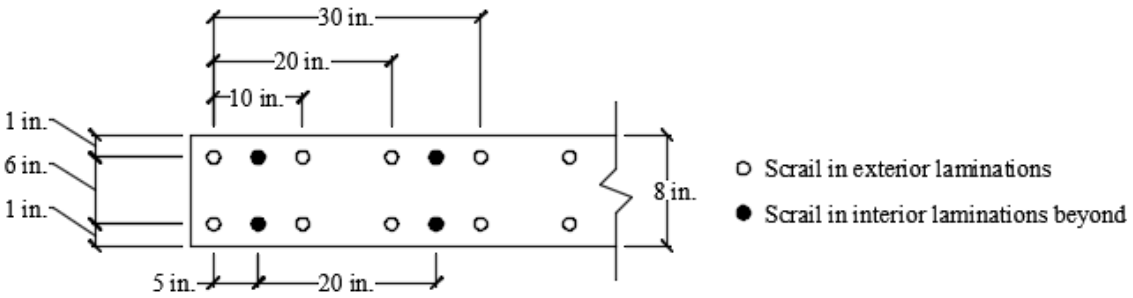

Figure 3.13. Elevation view of the fastener pattern for the 20° Plastic Strip Jumbo Scrails

Figure 3.14. Full size NLT mat being moved into the test setup

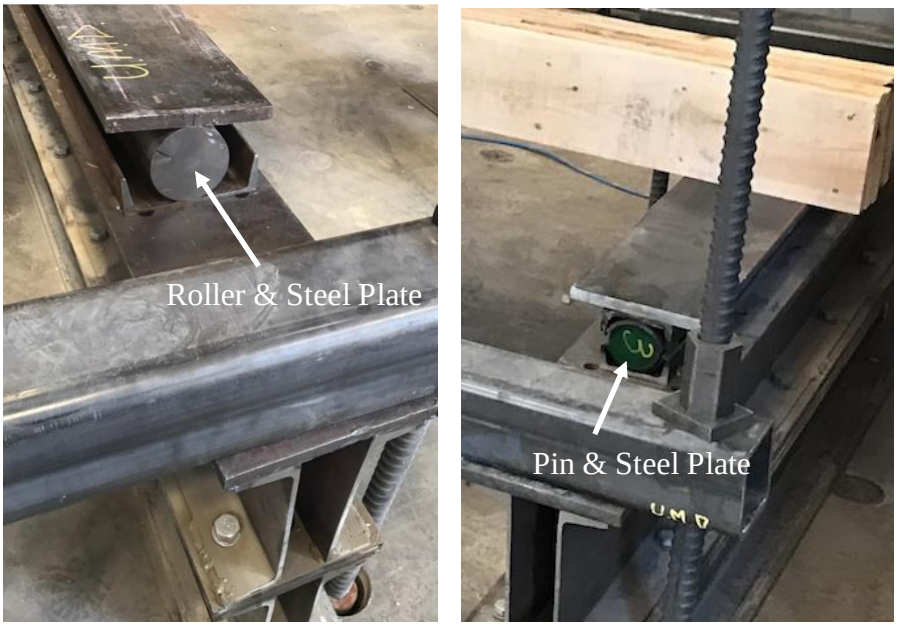

Figure 3.15. NLT support conditions in the UMD structures laboratory

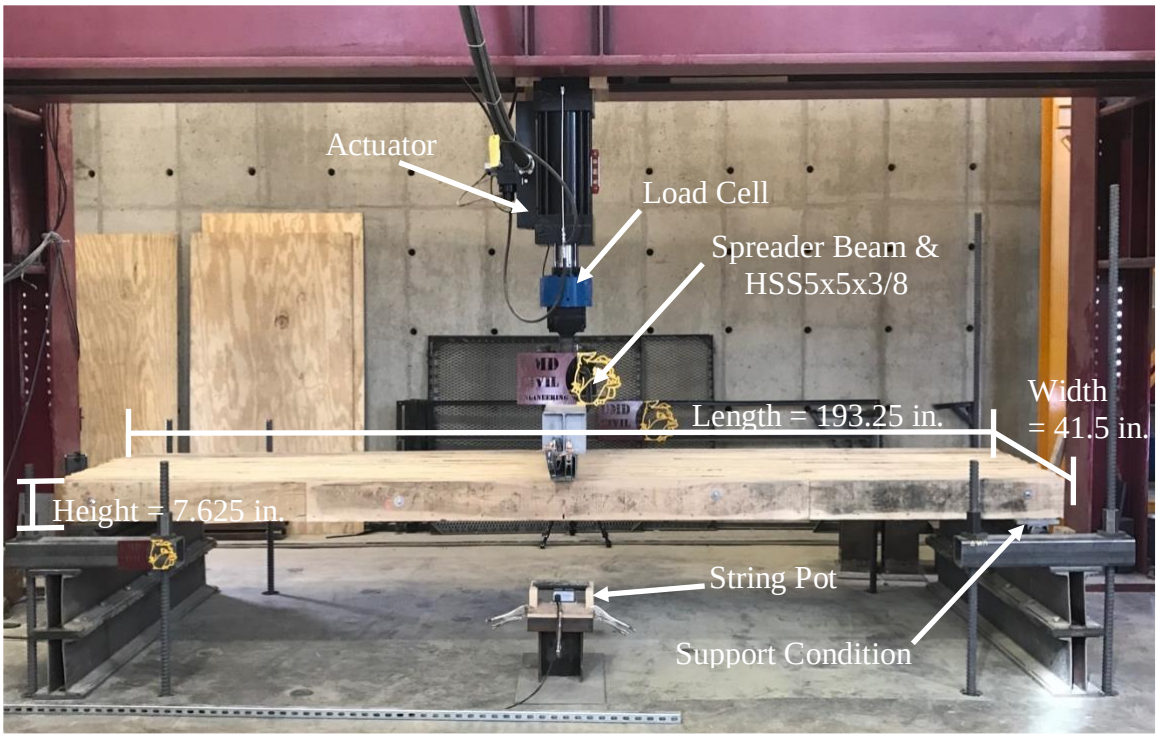

Figure 3.16. UMD test setup elevation with full size NLT specimen in position for testing

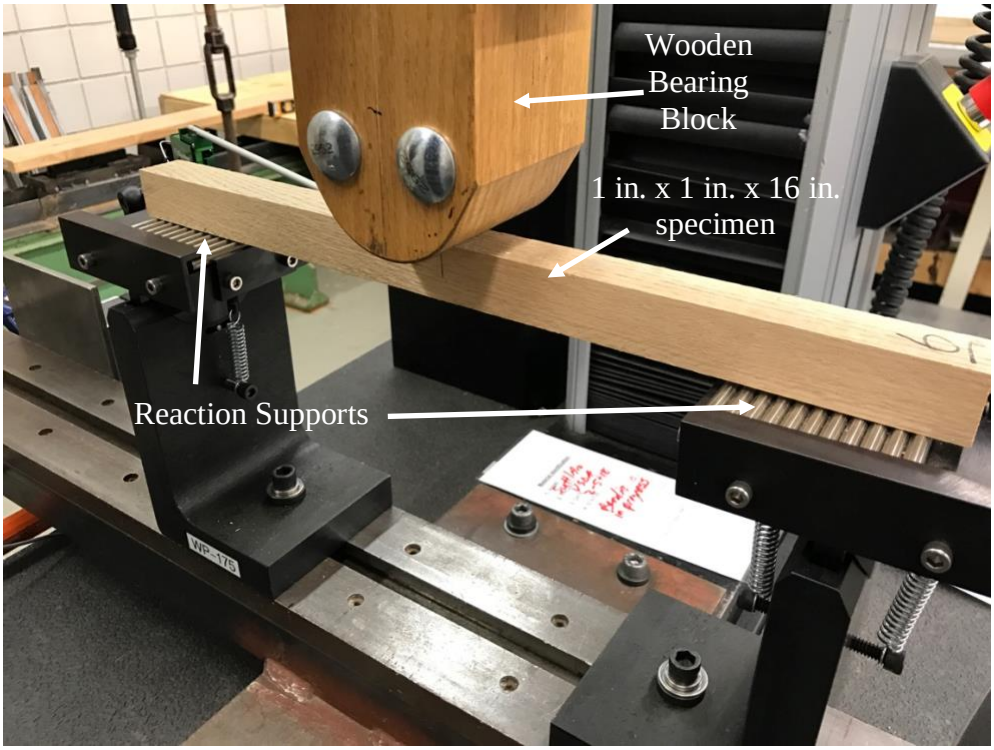

Figure 3.17. NRRI MOE test setup

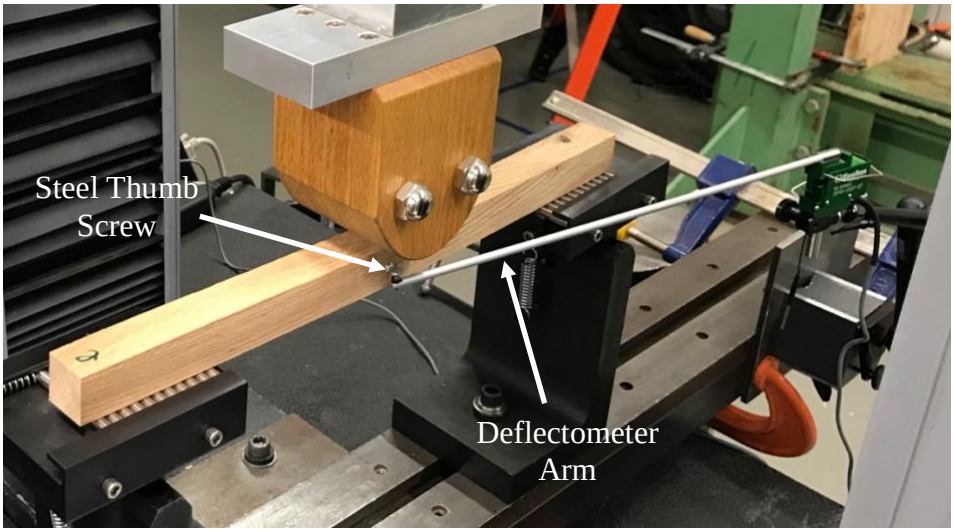

Figure 3.18. Deflectometer arm placed at midspan of the MOE specimen in the NRRI test setup

CHAPTER 4. TEST RESULTS, ANALYSIS, AND DISCUSSION

4.1 NRRI Material Properties

4.1.1 NRRI Modulus of Elasticity Test Results

The objective for testing the 16 in. long x 1 in. wide x 1 in. tall specimens at the NRRI was to quantify the MOE of the northern red oak lumber so it could be compared to the MOE of the NLT specimens that were tested at UMD. In order to determine the average MOE, the load vs. deflection curve for each of the 20 specimens was plotted on a single graph and a single linear trendline was fitted to the linear portion of the curves. The linear portion of the curve was defined as only the portion of the load vs. deflection curve between 10 and 30% of the peak load for each specimen. The slope of the trendline was used to determine the average apparent MOE, E_{app}, for the 20 specimens. The load vs. deflection curve for each of the 20 specimens and the associated linear trendline are shown in Figure 4.1. The equation that was used to calculate the apparent MOE in accordance with ASTM D198 (2015) is shown in Equation 4.1. The resulting average apparent MOE of the 20 specimens was approximately $6.38 * 10^5$ psi.

$$E_{app} = \frac{P * l^3}{4 * b * h^3 * \Delta} \quad 4.1$$

Immediately after testing, each specimen was examined to determine the failure mode in accordance with ASTM D198 (2015). All of the MOE specimens appeared to fail in a slow and ductile manner. Out of the 20 specimens, 80% exhibited a cross grain tension failure mode, where the fracture occurred due to a tensile force acting diagonally against the grain. A profile view of a typical cross grain tension failure is shown in Figure 4.2. The remaining 20% of the specimens exhibited a splintering tension failure mode, which consisted of a number of small tension failures on the bottom face of the specimen. A view of the tension surface after a typical splintering tension failure is shown in Figure 4.3.

4.1.2 Moisture Content

Five of the 16 in. long x 1 in. wide x 1 in. tall specimens were selected at random to determine the average moisture content of the northern red oak lumber used in this research. The moisture content of the five specimens ranged from 43% to 78% and had an average value of 56%. The moisture contents of the random samples are displayed in Table 4.1. Typically, dimensional lumber that is used for structural design is dried to provide a maximum moisture content of 19% when in service (NDS, 2018). It is expected that the moisture content will fluctuate substantially from mat to mat when using green northern red oak lumber to construct NLT crane mats. However, depending on the type of use in the field, crane mats are likely to be exposed to moist conditions that could exceed the standard moisture content of 19% that is used in structural design.

4.2 UMD Flexural Strength Testing

4.2.1 Experimental Flexural Test Results

All of the NLT specimens and the two solid timber beams displayed a ductile flexural failure. Load and deflection data for each test were graphed and analyzed to determine the maximum applied point load, corresponding deflection, and apparent MOE for each specimen. A summary of the maximum applied point load and corresponding deflection for each specimen is shown in Table 4.2. The apparent MOE of each specimen was determined by fitting a trendline to the linear portion of the applied load vs. deflection curve, which was between 10 and 30% of the maximum applied point load in accordance with ASTM D198 (2015). The slope of each trendline was used in Equation 4.1 to calculate the apparent MOE of each specimen. The applied load vs. deflection curves are shown in Figure 4.4 through Figure 4.14 and a summary of the apparent MOE of the test specimens is shown in Table 4.3. The following paragraphs describe the flexural test results for the solid timbers, nailed NLT beams, screwed NLT beams, scrailed NLT beams, and the 4 ft wide NLT mat.

The objective for testing the two solid timber beams was to form a baseline that could be compared to the flexural performance of the NLT specimens. The maximum point load applied to the solid timber specimens ranged from 5,176 to 7,629 lb and had an average value of 6,403 lb. The deflection exhibited by the solid timber specimens at the time of the peak load ranged from 4.06 to 5.85 in. and had an average value of 4.96 in. The

apparent MOE of the solid timber specimens ranged from $7.79*10^5$ to $1.19*10^6$ psi and had an average value of $9.85*10^5$ psi.

Three of the NLT beam specimens were constructed with 15° Wire Coil Nails. The maximum point load applied to the nailed NLT beam specimens ranged from 4,110 to 5,967 lb and had an average value of 5,258 lb. The average maximum applied point load for the nailed NLT beam specimens was approximately 82% of the average maximum applied point load exhibited by the solid timber specimens. The deflection exhibited by the nailed NLT beam specimens at the time of the peak load ranged from 3.27 to 4.26 in. and had an average value of 4.07 in. The apparent MOE of the nailed NLT beam specimens ranged from $7.71*10^5$ to $1.01*10^6$ psi and had an average value of $9.20*10^5$ psi.

Three of the NLT beam specimens were constructed with #12 x 5-5/8" R4™ Multi-Purpose Framing Screws. The maximum point load applied to the screwed NLT beam specimens ranged from 4,692 to 8,185 lb and had an average value of 5,937 lb. This was approximately 93% of the average maximum applied point load exhibited by the solid timber specimens. The deflection exhibited by the screwed NLT beam specimens at the time of the peak load ranged from 3.33 to 5.42 in. and had an average value of 3.67 in. The apparent MOE of the screwed NLT beam specimens ranged from $8.24*10^5$ to $1.09*10^6$ psi and had an average value of $9.17*10^5$ psi.

Two of the NLT beam specimens were constructed with 20° Plastic Strip Jumbo Scrails. The maximum point load applied to the scrailed NLT beam specimens ranged from 3,076 to 3,991 lb and had an average value of 3,534 lb. The maximum applied point load for the scrailed NLT beams was approximately 55% of the maximum applied point load displayed by the solid timber specimens. This was comparable to the results obtained by Bohnhoff et al. (1991), where NLT specimens with butt joints exhibited an average maximum applied point load that was approximately 45% of the average maximum applied point load for the NLT specimens that were constructed with all continuous laminations. The deflection exhibited by the scrailed NLT beam specimens at the time of the peak load ranged from 2.70 to 3.95 in. and had an average value of 3.30 in. The apparent MOE of the scrailed NLT beam specimens ranged from $6.78*10^5$ to $7.32*10^5$ psi and had an average value of $7.05*10^5$ psi. The average apparent MOE of the scrailed NLT beam specimens was approximately 72% of the average apparent MOE exhibited by the solid timber

specimens. This is similar to the results from Bohnhoff et al. (1991), where butt-jointed NLT specimens exhibited a bending stiffness that was approximately 60% of the bending stiffness for NLT specimens constructed with all continuous laminations.

Six of the NLT beam specimens were constructed with a random layup of laminations. The maximum point load applied to the random layup NLT beam specimens ranged from 4,110 to 8,185 lb and had an average value of 5,598 lb. This average maximum applied point load exhibited by the specimens constructed with random layups was approximately 87% of the average maximum applied point load for the solid timber specimens. The deflection exhibited by the random layup NLT beam specimens at the time of the peak load ranged from 3.27 to 5.42 in. and had an average value of 4.14 in. The apparent MOE of the random layup NLT beam specimens ranged from $7.71 * 10^5$ to $1.09 * 10^6$ psi and displayed an average value of $9.18 * 10^5$ psi.

Results for the NLT specimens constructed with a symmetric layup of laminations were identical to the results for the scrailed NLT beam specimens as they were the only specimens constructed with a symmetric layup. The average maximum applied point load for the specimens constructed with the symmetric layup was 77% of the maximum applied point load displayed by the specimens with random layups. This result agreed with the previous research performed by Haller (2000), which showed that a random layup of laminations provided greater flexural strength than NLT constructed with a consistent lamination layup. A potential reason for why the specimens constructed with a symmetric layup had a lower average maximum applied point load than the specimens constructed with random layups could be that the random pattern mitigates weak spots throughout the member, similar to oriented stand board (OSB). Another potential reason for the lower maximum applied point load of the symmetric layup specimens could be that the higher rigidity of the random layup specimens allowed for the load path to travel throughout the member more easily than symmetric layup specimens. This prevented the applied load from being concentrated on a smaller section of the specimen. A summary of the average NLT maximum applied point loads, deflections, and apparent MOEs based on fastener and layup type are shown in Table 4.4. The data in Table 4.4 are organized from the largest applied maximum load in the top row to the smallest applied maximum load in the bottom

row. However, there is no statistical significance of the results in Table 4.4 because of the small sample size of test specimens.

The Green, Scrailed NLT Mat performed as expected during testing because the maximum applied point load was approximately six times the magnitude of the maximum applied point loads exhibited by the individual scrailed NLT specimens. The maximum applied point load applied to the Green, Scrailed NLT mat was 23,547 lb. Standard crane operating weights can range from 20,000 to over 600,000 lb depending on the size of the crane and the load it is carrying. However, this weight is distributed through the wheels or tracks and outriggers, which makes it comparable to the maximum applied point load exhibited by the Green, Scrailed NLT Mat (23,547 lb). The maximum applied point load for the Green, Scrailed NLT Mat is shown in comparison to six times the maximum applied point loads for each of the individual NLT beam specimens in Figure 4.15. The deflection exhibited by the Green, Scrailed NLT Mat at the time of the maximum applied point load was 4.20 in. The apparent MOE of the Green, Scrailed NLT Mat was $7.04 * 10^5$ psi.

4.2.1.1 Discussion of Observed Failure Modes

The type of failure mode exhibited by each of the 11 specimens was documented immediately after testing. The NLT specimens failed in a much different fashion than the solid timber specimens due to the variability in butt joint locations, fastener types, and fastener patterns. The following paragraphs describe the types of failure observed during testing for the solid timbers, nailed NLT beams, screwed NLT beams, scrailed NLT beams, and the Green, Scrailed NLT Mat.

The Solid Timber (1) and (2) specimens both exhibited a cross grain tension failure as shown in Figure 4.16 and Figure 4.17, respectively. The Solid Timber (2) specimen displayed a large fracture originating from a knot that was within two feet of the applied point load as seen in Figure 4.17. This behavior indicated that the strength was affected by the defect, which may explain why the maximum point load applied to the Solid Timber (2) specimen was significantly less than that of the Solid Timber (1).

The nailed NLT specimens exhibited a variety of failure modes, unlike the single type of failure observed in each of the solid timber specimens. The Dried, Nailed NLT (1) specimen displayed a tension failure in all of the three interior laminations that were continuous underneath the point of loading as shown in Figure 4.18. Additionally, a

compression failure at one of the two butt joints located directly beneath the load was observed in the same specimen. Figure 4.19 shows a typical compression failure at a butt joint where crushing of the wood directly under the load had occurred and the pieces of lumber on either side of the joint were displaced downward. The Dried, Nailed NLT (2) specimen exhibited a splintering tension failure in one of the laminations that was continuous under the load as well as compression failures at both of the butt joints located at midspan. The Green, Nailed NLT specimen displayed both splintering tension failures and compression failures comparable to the previous specimens, however, an additional compression failure at one of the butt joints located approximately two feet from midspan was observed. Fasteners were pulled through the exterior lamination on one side of the butt joint and entirely disconnected from the lamination as shown in Figure 4.20. This could be the reason that the capacity of the Green, Nailed NLT specimen was lower when compared to the Dried, Nailed NLT (1) and (2) specimens.

The screwed NLT specimens exhibited failure modes that were similar to the Dried, Nailed NLT (1) specimen, but slightly more dramatic. Two of the interior laminations of the Dried, Screwed NLT (1) specimen that were continuous underneath the load exhibited a cross grain tension failure on the bottom surface, exposing nails in the bottom row of the fastener pattern as shown in Figure 4.21. The two laminations that contained butt joints at the location of the load and one laminated with a butt joint located 2 ft from the load displayed a compression failure. The Dried, Screwed NLT (2) specimen exhibited similar behavior to the Dried, Screwed NLT (1) specimen. In this case, large cracks were observed in the exterior laminations that originated at the butt joints and formed parallel to the grain of the wood as shown in Figure 4.22. The Green, Screwed NLT specimen also exhibited a splintering tension failure in the four laminations that were continuous under the load as well as compression failures at the butt joints as shown in Figure 4.23. A significant amount of cracking was visible at butt joints in the exterior laminations, which extended toward the location of loading similar to that shown in Figure 4.22.

The scrailed NLT beam specimens exhibited comparable failure modes to both the nailed and screwed NLT specimens. Both tension and compression failures were observed. The Green, Scrailed NLT (1) specimen showed splintering tension failures in the four continuous laminations under the load, but the cracks propagated toward a nearby knot in

one of the laminations as shown in Figure 4.24. Additionally, both of the laminations containing butt joints two feet from the location of the applied load experienced a compression failure that separated the ends of the individual pieces of lumber from the adjacent laminations. This combination of splintering tension and compression could have caused premature failure, resulting in the low magnitude point load that was observed just before failure in the Green, Scrailed NLT (1) specimen. The Green, Scrailed NLT (2) specimen exhibited cross grain tension failures in the exterior laminations comparable to the failure observed in the Dried, Nailed NLT (1) specimen. Compression failures in one of the two butt joints directly underneath the load was also observed.

The 4 ft wide Green, Scrailed NLT Mat specimen exhibited a failure mode that was significantly different from the smaller NLT beam specimens. In this case, a tension failure was observed at the exterior laminations, where cracking began near the bottom of the specimen and propagated outward from the point load as shown in Figure 4.25. The interior laminations appeared to fail due to splintering and cross grain tension. There were no visible compression failures occurring at any of the butt joint locations. This behavior could be caused by the additional composite action that was created by the four threaded rods, which held the six individual NLT beams together. This general observation suggests that the Green, Scrailed NLT Mat behaved more closely to a solid structural element than any of the individual NLT beams.

In general, all of the NLT beam specimens exhibited a tension failure in at least one of the laminations that were continuous under the location of the applied load. Additionally, at least one of the two butt joints located under the applied load displayed a compression failure for all of the NLT beam specimens. This was similar to the results obtained by Winistorfer et al. (1987), where the NLT test specimens generally exhibited tension failure in individual laminations and compression failure at the butt joints. Two of the eight NLT beams (the Green, Nailed NLT and Green, Scrailed NLT (1) specimens) also exhibited compression failures at butt joints that were located two feet from the location of the applied load. The 4 ft wide Green, Scrailed NLT Mat specimen exhibited a tension failure in the laminations that were continuous under the applied load that was similar to the NLT beam specimens. However, the Green, Scrailed NLT Mat did not show signs of a compression failure at any of the butt joints in the laminations.

4.2.2 Theoretical Flexural Strength Predictions

4.2.2.1 Assumptions for Capacity Predictions

The IBC (2018) and NLT Design Guide (2017) flexural strength equations were used to predict the capacity of each NLT specimen. Both of these methods incorporate the reference bending design value (F_b), which is multiplied by a series of adjustment factors as specified by the NDS for Wood Construction (2018) as shown in Equation 2.1. In order to provide accurate results that would best represent the test setup and specimens in this research, a number of assumptions were made for the applicable adjustment factors.

Reference bending design values were first adjusted using a load duration factor, C_d, based on the type of loading (ranging from dead to impact loads). Because tests performed in this research occurred over a short period of time, with the load applied at a much faster pace than typical vertical building loads, the type of loading was considered to be most closely related to a construction load. This resulted in a load duration factor of 1.25. A higher value would only be used in cases were seismic or impact loading was expected. The second adjustment factor that was applied to the reference bending design value was the wet service factor, C_M. When the moisture content of the lumber exceeds 19%, the wet service factor is equal to a value of 0.85 for determining the bending strength and 0.9 for calculating the adjusted MOE. This was justified by the results from the MOE test at the NRRI, which indicated that the northern red oak had an average moisture content of 56%. Although four of the NLT specimens were dried to a lower moisture content, it was expected to still be greater than 19%. The temperature adjustment factor, C_t, was assumed to have a value of 1.0 as the test specimens were not exposed to temperatures over 100°F. The beam stability factor, C_L, was applied to the reference bending design value and was taken as a value of 1.0 because the width of the test specimens was typically equal to or greater than the depth of the member, which provided adequate lateral stability. The size factor, C_F, was determined to be 1.2 according to the tabulated values for dimensional lumber having a nominal depth of 8 in. in the NDS Supplement (2018). A flat use factor, C_{fu}, is often included in the adjustments made to the reference bending design value when the lumber is loaded on the wide face. In this case, the lumber was loaded on the smaller face (stronger axis), which justified a value of 1.0 for this adjustment factor. The incising factor, C_i, was also taken as 1.0 because there were no cuts or changes in the section

throughout the length of each member. A repetitive member factor, C_r, was applied in accordance with the NDS for Wood Construction (2018). When members are spaced less than or equal to 24 in. o.c., this adjustment factor is assumed to be 1.15. Because each lamination of lumber in NLT is fastened to the adjacent laminations, a value of 1.15 was practical for the repetitive member factor.

Theoretical flexural strength predictions were also estimated for the two solid timber beams that were tested with the NLT specimens. These predictions were based solely on the NDS for Wood Construction (2018). Sample calculations for flexural strength predictions of the solid timber beams are shown in Appendix B.1. The assumptions made for the reference bending design value adjustment factors were almost identical to those made for the NLT specimens but differed for the wet use, size, and the repetitive member factors. When solid timbers that are 5 in. x 5 in. or larger are used where the moisture content will exceed 19%, the wet service factor is specified as 1.0 for adjustment to both the reference bending and MOE design values in accordance with the NDS for Wood Construction (2018). The size factor for the solid timbers was also assumed to be 1.0 as the specimens were greater than 4 in. thick and had a depth less than 12 in. in accordance with the NDS for Wood Construction (2018). The repetitive member factor is only applicable to dimensional lumber up to 4 in. thick, therefore, a value of 1.0 was assumed for the solid timber strength predictions.

In general, reference bending design values tabulated in the NDS for Wood Construction (2018) are determined based on ASTM tests. To account for the effects of the natural growth characteristics of the wood, a reduction factor known as a strength ratio is applied to the measured strength values prior to acceptance by the NDS for Wood Construction. Additionally, the values are further reduced by a general adjustment factor, which accounts for the duration of the test used to establish the design values, manufacturing adjustments, and the type of use according to the Design of Wood Structures ASD/LRFD Seventh Edition (2015). The combined effects of these reductions is intended to provide an average safety factor of 2.5 (Design of Wood Structures, 2015). Due to the large number of variables in wood design, safety factors may range from 1.25 to 5.0. In order to provide strength predictions that would best represent the behavior of the lumber

used in this research, reference bending design values were multiplied by an average safety factor of 2.5 for comparison to experimental results.

4.2.2.2 International Building Code Method

The IBC (2018) specifies a design equation to determine the allowable area load for flexure, σ_b, for NLT. However, this equation is only applicable to members that have three spans and a uniformly distributed applied load over the entire three-span member. In order to relate the IBC (2018) design methodology to the three point bending setup used for testing in this research, the origin of the allowable area load equation was determined. The allowable area load equation for flexure was derived for a continuous beam with three equal spans and a uniform load applied across the entire beam using structural analysis. This three-span continuous beam with uniform loading was used as the reference design starting with the American Institute of Timber Construction (AITC) 112-93 Standard (AITC, 1993). Additionally, a safety factor of 0.66 was applied to the equation based on previous research (Currier, 1955) and the presence of this safety factor was verified by the American Wood Council (Koch, 2018). A detailed derivation of the IBC (2018) allowable area load for flexure is shown in Appendix B.2. In lieu of this, a similar equation for σ_b was derived following the same methodology but for a simply supported beam with a single point load applied at midspan (three point bending). Rather than resulting in a stress over the length and width of the member in psi, the derivation produced an allowable point load that was distributed across the width of the member at midspan in plf, which is referred to as the allowable distributed point load and denoted by σ_p. The derived equation for the allowable distributed point load is shown in Equation 4.2.

$$\sigma_p = \frac{2 * F_b' * d^2}{3 * l} \tag{4.2}$$

In this case, the safety factor of 0.66 was excluded as there was no obvious justification for its relevancy to a simply supported beam condition with a point load at midspan. A detailed derivation of the allowable distributed point load (σ_b) is shown immediately following the derivation of the IBC (2018) allowable area load equation (σ_b) in Appendix B.2.

The derived equation for allowable point load at midspan was used to predict the IBC flexural capacity for each of the NLT specimens. Calculations were performed using reference design values for all grades of northern red oak dimensional lumber that are tabulated in the NDS for Wood Construction (2018) because the design values for the rough cut northern red oak lumber used in this testing were unknown. The predicted maximum applied point loads for each NLT specimen were then compared to the experimental maximum applied point load results to determine which grade was validated by the experimental results. This was achieved by calculating a ratio of the theoretical point load to the experimental point load for each grade and specimen. The ratios were averaged for each grade of lumber. The theoretical point loads, experimental point loads, and ratios of the two are shown in Table 4.5 and Table 4.6. Stud grade lumber produced an average ratio of 0.89, which was the closest to unity considering all of the possible grades. This indicated that using stud grade lumber for theoretical predictions provided the closest results to experimentally measured maximum applied point loads. Sample calculations for the flexural strength of each NLT specimen using stud grade reference design values are shown in Appendix B.3. The reference design values for bending (F_b = 750 psi) and modulus of elasticity ($E = 1.2{*}10^6$ psi) for stud grade lumber, which are tabulated in the NDS for Wood Construction (2018), were used for all theoretical NLT flexural strength predictions in order to compare results between different flexural strength prediction methods.

4.2.2.3 NLT Design Guide Method

The NLT Design Guide (2017) was used to predict the flexural strength for all of the NLT specimens. This method is almost identical to the allowable distributed point load function shown in equation 4.2. However, it includes additional adjustment factors based on the cross section and layup of the NLT as previously described in Section 2.1.3 of this report. Additionally, the NLT Design Guide (2017) was used to predict the MOE for all of the NLT specimens using Equation 2.7. The NLT Design Guide (2017) specifies equations for predicting the expected deflection, but the equations are only suitable for loads that are uniformly distributed across the entire span of the member. For simplicity, The AISC Manual (2015) was used to determine deflections using the NLT modulus of elasticity, E'_{NLT}. Specifically, the maximum deflection was predicted using a simply supported beam

condition with a single point load applied at midspan. The equation used to predict the maximum deflection is shown in Equation 4.3.

$$\Delta_{max} = \frac{P * l^3}{48 * E'_{NLT} * I} \quad 4.3$$

The moment of inertia, *I*, was calculated by multiplying 1/12 by the entire width of the NLT member and by the depth of the NLT member to the third power. A summary of the theoretical peak load, MOE, and deflection for all of the NLT specimens using the NLT Design Guide (2018) is shown in Table 4.7. The reference design values for bending (F_b = 750 psi) and modulus of elasticity (E =1.2∗10^6 psi) for stud grade lumber were used in all of the NLT Design Guide (2017) calculations. Sample calculations for maximum applied point load, MOE, and deflection can be found in Appendix B.4.

4.2.3 Comparison of Theoretical and Experimental Test Results and Discussion

The goal of comparing the theoretical and experimental results was to determine if the current NLT design methods would be applicable to the beams tested in this research and basic NLT crane mat design. In general, the theoretical results for maximum applied point load, MOE, and deflection were conservative compared to the experimental NLT results.

The maximum allowable loads determined using the IBC (2018) method were conservative for all of the nailed and screwed NLT specimens. However, this method proved unconservative for the Green, Scrailed NLT (1), Green Scrailed NLT (2), and Green, Scrailed NLT Mat specimens. A summary of the experimental (Exp.) maximum applied point loads and theoretical (Theo.) maximum applied point loads is listed in Table 4.8. On average, the IBC (2018) method yielded maximum applied point loads that were approximately 28% less than the experimental maximum applied point loads for the nailed and screwed NLT specimens (calculated by dividing the IBC average maximum applied point load by the average of the maximum applied point loads for the nailed and screwed NLT specimens in Table 4.8 and converting to a percentage). The theoretical maximum applied point loads for the scrailed specimens were 8% greater than the experimental test results. The NLT Design Guide (2017) results were more conservative than the IBC (2018)

method when using the same reference bending design values for stud grade lumber. The NLT Design Guide (2017) predictions resulted in maximum allowable loads that were less than all of the experimental results. On average, the NLT Design Guide (2017) predictions for maximum applied point load were only 26% of the experimental values (very conservative). This was calculated by dividing the average maximum applied point loads for the NLT Design Guide by the average maximum applied point load of all of the NLT specimens in Table 4.8 and converting to a percentage. Differences in maximum applied point load results between the two theoretical methods is likely due to the inclusion of the layup factor for bending ($K_{layup.b}$) in the NLT Design Guide (2017) method. The additional adjustment factor is used to limit the design capacity of NLT based on effects due to fastener and lamination layup patterns, but in this case resulted in extremely conservative values.

Theoretical predictions for MOE using the NLT Design Guide (2017) were conservative in comparison to the average apparent MOE for all of the NLT specimens. A summary of the values for the experimental NLT MOE, the MOE obtained from testing at the NRRI, and the theoretical MOE is shown in Table 4.9. On average, the theoretical results for MOE were approximately 65% of the measured values from testing (calculated by dividing the average MOE for the NLT Design Guide by the average experimental MOE in Table 4.9 and converting to a percentage). Theoretical predictions for MOE fitted more closely with the results from the NRRI MOE testing compared to the experimental results for MOE of the NLT specimens. The average of the predicted NLT MOE values was approximately 86% of that obtained from the NRRI MOE test results (calculated by dividing the average MOE for the NLT Design Guide by the NRRI MOE in Table 4.9 and converting to a percentage). The MOE obtained through testing at the NRRI was consistently conservative in comparison to the experimentally measured NLT MOE results. This indicated that all of the NLT specimens exhibited a higher stiffness than the individual northern red oak lumber specimens.

Experimentally measured deflections of the NLT specimens were significantly greater than the theoretical deflections that were calculated using Equation 4.3. On average, the theoretical deflections were 27% of the deflections exhibited by the NLT when the maximum load was applied. Theoretical predictions for deflection were most similar to the

deflections exhibited by the scrailed NLT specimens but were still only 29% of the experimentally measured values. The large difference between these results was likely due to the fact that Equation 4.3 does not account for the effects of the fastener types, fastener patterns, or layup types used in the NLT. These effects would need to be thoroughly understood in order to provide more accurate predictions. Experimental results and theoretical predictions for NLT deflections are summarized in Table 4.10.

4.3 Crane Mat Cost Analysis

A cost analysis covering the life span of each type of NLT crane mat (e.g., nailed, screwed, or scrailed) was performed to investigate if production would be economically feasible. The cost of manufacturing, transportation, and disposal were considered in determining the total cost of a 4 ft wide x 8 in. deep x 16 ft long crane mat that would be fastened together with either nails, screws, or scrails. The cost of materials and labor associated with constructing the crane mats was provided by Savanna Pallets, Inc. and the NRRI. The cost of materials and labor associated with constructing a crane mat ranged from $564.24 to $603.60 depending on the type of fastener used.

Energy usage involved with constructing a 4 ft wide x 8 in. deep x 16 ft long NLT crane mat was determined according to the Minnesota Power Electricity Rate Book (2009). A commercial electricity rate of 7.836 cents/kWh was used to calculate the energy costs associated with cutting the lumber to size, fastening the individual laminations together, and installing the threaded rods in each crane mat. Energy usage for the various equipment involved with these tasks (e.g., a table saw, corded drill, and nail gun) was determined according to standard appliance energy rates published in the Payson City Corporation Energy Use Charts (2018). The energy rates were multiplied by the estimated time to complete each task and the commercial electricity rate of 7.836 cents/kWh in order to calculate a total cost of electricity usage. The time to perform each task was estimated based on the time required to manufacture the specimens described in this research. Typically, additional costs for drying the lumber and disposing of any byproduct or waste would be included in construction costs. However, these items were disregarded as Savanna Pallets, Inc. chose to use green northern red oak lumber and any byproduct would be ground up and sold as mulch or animal bedding. Drying lumber and grinding and selling any byproduct would result in an additional costs and gains associated with the total crane

mat production costs. The total cost of energy to fabricate a single NLT crane mat fastened together with nails, screws, or scrails was $0.13, $0.03, and $0.06, respectively.

The cost of transportation and landfilling associated with disposing of an NLT crane mat was determined using average costs in the Midwestern U.S. The use of mechanical fasteners for connecting individual laminations of lumber prevented the possibility of recycling a crane mat after it had reached the end of its life because all of the fasteners would need to be removed from the lumber before it could be chipped and disposed of. The cost of transportation to a landfill may vary significantly depending on the location of the project site. To provide a general estimate, a distance of 100 miles was used in determining disposal costs. According to DAT Solutions (2018), the average shipping cost per mile for a flatbed truck in the Midwestern U.S. was $3.14, which resulted in the total transportation cost of approximately $314.00. However, this cost would likely decrease over time because more than one crane mat can be transported on a single flatbed truck. As of 2016, landfill costs averaged approximately $48.40 per ton of waste in the Midwest according the Solid Waste Environmental Excellence Protocol (2016). With an estimated weight of 1,500 lb (0.75 ton) per mat, the landfilling cost for a single NLT crane mat would be $36.30. This resulted in a total disposal cost of approximately $350.30. However, if these 4 ft wide crane mats were mass produced, disposing a large volume of them would become impractical due to the extensive landfilling process required.

The intent of this project was to provide Savanna Pallets, Inc. with economical NLT designs that could be put into mass production. Savanna Pallets, Inc. provided potential customers with a series of field prototypes to better understand the wearing patterns and structural challenges of designing a crane mat prior to any laboratory testing. At this time, the question of disposal was raised and it became clear that this was a critical barrier to market entry. Savanna Pallets, Inc. and the NRRI determined that the final crane mat design was not adequate for mass fabrication as there would be an unreasonable economic burden placed on the utility companies who procured the product to dispose of mats fabricated with metal fasteners. This limitation was not defined in the initial planning stages of this project.

The total cost for a 4 ft wide x 8 in. deep x 16 ft long NLT crane mat fastened together with nails, screws, and scrails was $914.66, $929.44, and $953.95 respectively.

The differences in total cost depended solely on the type of fastener used. A detailed breakdown of the costs associated with materials, energy usage, transportation, and disposal of the NLT crane mats is shown in Appendix C and reflected in Table 4.11. Commercial prices of crane mats can vary considerably depending on the type and size. Price quotes were obtained via email from Spartan Mat LLC and Viking Mat Co. to compare NLT crane mat costs to those currently used in industry. The price of one 4 ft wide x 8 in. deep x 16 ft long solid timber crane mat from Spartan Mat LLC was quoted at $4,000.00, including shipping. Additionally, a single 4 ft wide x 12 in. deep x 16 ft long solid timber crane mat from Viking Mat Co. was priced at $3,550.00. These were the costs to purchase a crane mat rather than just the construction and disposal costs for the manufacturer. The cost of the NLT crane mats fabricated in this study were a fraction of the cost of those provided by manufacturers in the industry. However, 4 ft wide x 8 in. deep x 16 ft long solid timber crane mats may cost as low as $350.00 to purchase depending on the volume and customer demand (Koen, 2018), which is less than the cost to manufacture a single NLT crane mat.

Table 4.1. Wet weight, dry weight, and moisture content of the random samples tested at the NRRI

Random Sample #	Wet Weight (g)	Dry Weight (g)	Moisture Content (%)
1	18.65	13.06	42.8
2	16.44	11.19	46.9
3	17.49	10.82	61.6
4	19.02	12.61	50.8
5	13.51	7.59	78.0
		Average:	**56.0**

Table 4.2. Maximum applied point load and corresponding midspan deflection for each of the NLT specimens tested at UMD

Specimen	Maximum Applied Point Load (lb)	Midspan Deflection at Maximum Applied Point Load (in.)
Solid Timber (1)	7,629	5.85
Solid Timber (2)	5,176	4.06
Dried, Nailed NLT (1)	5,967	4.07
Dried, Nailed NLT (2)	5,698	3.27
Dried, Screwed NLT (1)	4,692	3.33
Dried, Screwed NLT (2)	8,185	5.42
Green, Nailed NLT	4,110	4.26
Green, Screwed NLT	4,933	4.48
Green, Scrailed NLT (1)	3,076	2.70
Green, Scrailed NLT (2)	3,991	3.95
Green, Scrailed NLT Mat	23,547	4.20

Table 4.3. Apparent MOE for two solid timber and nine NLT specimens

Specimen	**Slope = $\frac{P}{\Delta}$ (kip/in.)**	**Width (in.)**	**Depth (in.)**	**Length (in.)**	**E_{app} (psi)**
Solid Timber (1)	2.30	7.375	7.25	180	$1.19*10^6$
Solid Timber (2)	1.69	7.5	7.5	180	$7.79*10^5$
Dried, Nailed NLT (1)	1.84	8.0	7.0	180	$9.78*10^5$
Dried, Nailed NLT (2)	1.98	8.0	7.125	180	$1.01*10^6$
Dried, Screwed NLT (1)	1.66	7.875	7.125	180	$8.36*10^5$
Dried, Screwed NLT (2)	1.75	8.125	7.25	180	$8.24*10^5$
Green, Nailed NLT	1.59	7.125	7.5	180	$7.71*10^5$
Green, Screwed NLT	1.85	7.625	6.875	180	$1.09*10^6$
Green, Scrailed NLT (1)	1.53	6.875	7.625	180	$7.32*10^5$
Green, Scrailed NLT (2)	1.59	7.0	7.875	180	$6.78*10^5$
Green, Scrailed NLT Mat	8.88	41.5	7.625	180	$7.04*10^5$
				Average:	**$8.72*10^5$**

Table 4.4. Average maximum applied point load, deflection and MOE for NLT beam specimens based on fastener and layup type

Type of Specimen	**Number of Specimens**	**Average Maximum Applied Point Load (lb)**	**Average Deflection at Maximum Applied Point Load (in.)**	**Average Modulus of Elasticity (psi)**
Solid Timber	2	6,403	4.96	$9.85*10^5$
Screwed NLT	3	5,937	4.41	$9.17*10^5$
Random Layup NLT	6	5,598	4.14	$9.18*10^5$
Nailed NLT	3	5,258	3.87	$9.20*10^5$
Scrailed NLT	2	3,534	3.33	$7.05*10^5$
Symmetric Layup NLT	2	3,534	3.33	$7.05*10^5$

Table 4.5. Experimental (Exp.) and theoretical (Theo.) maximum applied point loads based on the IBC (2018) using utility, standard, construction, and stud grade lumbers

Specimen	**Exp. Point Load (lb)**	**Lumber Grade**							
		Utility (F_b = 300 psi)		**Standard (F_b = 625 psi)**		**Construction (F_b = 1100 psi)**		**Stud (F_b = 750 psi)**	
		Theo. Point Load (lb)	**Theo. / Exp.**	**Theo. Point Load (lb)**	**Theo. / Exp.**	**Theo. Point Load (lb)**	**Theo. / Exp.**	**Theo. Point Load (lb)**	**Theo. / Exp.**
Dried, Nailed NLT (1)	5,967	1,597	0.27	3,326	0.56	5,854	0.98	3,991	0.67
Dried, Nailed NLT (2)	5,698	1,628	0.29	3,392	0.60	5,970	1.05	4,071	0.71
Dried, Screwed NLT (1)	4,692	1,654	0.35	3,446	0.73	6,065	1.29	4,135	0.88
Dried, Screwed NLT (2)	8,185	1,739	0.21	3,624	0.44	6,378	0.78	4,349	0.53
Green, Nailed NLT	4,110	1,632	0.40	3,401	0.83	5,985	1.46	4,081	0.99
Green, Screwed NLT	4,933	1,468	0.30	3,058	0.62	5,382	1.09	3,670	0.74
Green, Scrailed NLT (1)	3,076	1,598	0.52	3,330	1.08	5,861	1.91	3,996	1.30
Green, Scrailed NLT (2)	3,991	1,737	0.44	3,608	0.90	6,367	1.60	4,341	1.09
Green, Scrailed NLT Mat	23,547	9,886	0.42	20,597	0.87	36,250	1.54	24,716	1.05
Average:	7,133	2,549	**0.35**	5,309	**0.74**	9,346	**1.30**	6,372	**0.89**

Table 4.6. Experimental (Exp.) and theoretical (Theo.) maximum applied point loads based on the IBC (2018) using No. 3, No. 2, No.1 and Select Structural grade lumbers

Specimen	Exp. Point Load (lb)	Lumber Grade							
		No. 3 (F_b = 550 psi)		No. 2 (F_b = 975 psi)		No. 1 (F_b = 1000 psi)		Select Structural (F_b = 1400 psi)	
		Theo. Point Load (lb)	Theo. / Exp.	Theo. Point Load (lb)	Theo. / Exp.	Theo. Point Load (lb)	Theo. / Exp.	Theo. Point Load (lb)	Theo. / Exp.
Dried, Nailed NLT (1)	5,967	2,927	0.49	5,189	0.87	5,322	0.89	7,451	1.25
Dried, Nailed NLT (2)	5,698	2,985	0.52	5,292	0.93	5,428	0.95	7,599	1.33
Dried, Screwed NLT (1)	4,692	3,033	0.65	5,376	1.15	5,514	1.18	7,719	1.65
Dried, Screwed NLT (2)	8,185	3,189	0.39	5,653	0.69	5,798	0.71	8,117	0.99
Green, Nailed NLT	4,110	2,993	0.73	5,305	1.29	5,441	1.32	7,618	1.85
Green, Screwed NLT	4933	2,691	0.55	4,771	0.97	4,893	0.99	6,850	1.39
Green, Scrailed NLT (1)	3,076	2930	0.95	5,195	1.69	5,328	1.73	7,459	2.42
Green, Scrailed NLT (2)	3,991	3,184	0.80	5,644	1.41	5,788	1.45	8,104	2.03
Green, Scrailed NLT Mat	23,547	18,125	0.77	32,131	1.36	32,955	1.40	46,137	1.96
Average:	7,133	4,673	**0.65**	8,284	**1.15**	8,496	**1.18**	11,895	**1.65**

Table 4.7. NLT Design Guide (2017) theoretical (Theo.) maximum applied point load, MOE, and deflection for each of the NLT specimens using stud grade lumber

Specimen	Stud Grade Lumber (F_b = 750 psi)		
	Theo. Maximum Applied Point Load (lb)	**Modulus of Elasticity (psi)**	**Deflection (in.)**
Dried, Nailed NLT (1)	1,230	$6.92*10^5$	0.94
Dried, Nailed NLT (2)	1,249	$6.81*10^5$	0.94
Dried, Screwed NLT (1)	1,182	$6.34*10^5$	0.94
Dried, Screwed NLT (2)	1,237	$6.24*10^5$	0.93
Green, Nailed NLT	1,236	$6.50*10^5$	0.92
Green, Screwed NLT	1,058	$6.55*10^5$	0.95
Green, Scrailed NLT (1)	1,123	$5.96*10^5$	0.92
Green, Scrailed NLT (2)	1,210	$5.79*10^5$	0.91
Average Without NLT Mat:	**1,190**	$\mathbf{6.39*10^5}$	**0.93**
Green, Scrailed NLT Mat	6,944	$5.96*10^5$	0.92
Average With NLT Mat:	**1,830**	$\mathbf{6.34*10^5}$	**0.93**

Table 4.8. Experimental maximum applied point loads and theoretical maximum applied point loads using the IBC (2018) and the NLT Design Guide (2017)

Specimen	**Maximum Applied Point Load (lb)**		
	Experimental	**IBC (2018)**	**NLT Design Guide (2017)**
Solid Timber (1)	7,629	-	-
Solid Timber (2)	5,176	-	-
Dried, Nailed NLT (1)	5,967	3,991	1,230
Dried, Nailed NLT (2)	5,698	4,071	1,249
Dried, Screwed NLT (1)	4,692	4,135	1,182
Dried, Screwed NLT (2)	8,185	4,349	1,237
Green, Nailed NLT	4,110	4,081	1,236
Green, Screwed NLT	4,933	3,670	1,058
Green, Scrailed NLT (1)	3,076	3,996	1,123
Green, Scrailed NLT (2)	3,991	4,341	1,210
Average Without NLT Mat:	**5,082**	**4,079**	**1,191**
Green, Scrailed NLT Mat	23,547	24,716	6,944
Average With NLT Mat:	**7,133**	**6,372**	**1,830**

Table 4.9. Experimental MOE, NRRI MOE, and theoretical MOE using the NLT Design Guide (2017)

Specimen	**Modulus of Elasticity (psi)**		
	Experimental	**NRRI**	**NLT Design Guide (2017), E'_{NLT}**
Solid Timber (1)	$1.19*10^6$	$6.38*10^5$	-
Solid Timber (2)	$7.79*10^5$	$6.38*10^5$	-
Dried, Nailed NLT (1)	$9.78*10^5$	$6.38*10^5$	$5.93*10^5$
Dried, Nailed NLT (2)	$1.01*10^6$	$6.38*10^5$	$5.84*10^5$
Dried, Screwed NLT (1)	$8.36*10^5$	$6.38*10^5$	$5.43*10^5$
Dried, Screwed NLT (2)	$8.24*10^5$	$6.38*10^5$	$5.35*10^5$
Green, Nailed NLT	$7.71*10^5$	$6.38*10^5$	$5.57*10^5$
Green, Screwed NLT	$1.09*10^6$	$6.38*10^5$	$5.61*10^5$
Green, Scrailed NLT (1)	$7.32*10^5$	$6.38*10^5$	$5.11*10^5$
Green, Scrailed NLT (2)	$6.78*10^5$	$6.38*10^5$	$4.97*10^5$
Average Without NLT Mat:	$\mathbf{8.65*10^5}$	$\mathbf{6.38*10^5}$	$\mathbf{5.48*10^5}$
Green, Scrailed NLT Mat	$7.04*10^5$	$6.38*10^5$	$5.11*10^5$
Average With NLT Mat:	$\mathbf{8.47*10^5}$	$\mathbf{6.38*10^5}$	$\mathbf{5.47*10^5}$

Table 4.10. Experimental deflections and theoretical deflections calculated using Equation 4.3

Specimen	Experimental Deflection (in.)	Theoretical Deflection (in.)
Solid Timber (1)	5.85	2.42
Solid Timber (2)	4.06	2.34
Dried, Nailed NLT (1)	4.07	1.10
Dried, Nailed NLT (2)	3.27	1.10
Dried, Screwed NLT (1)	3.33	1.10
Dried, Screwed NLT (2)	5.42	1.09
Green, Nailed NLT	4.26	1.08
Green, Screwed NLT	4.48	1.11
Green, Scrailed NLT (1)	2.70	1.07
Green, Scrailed NLT (2)	3.95	1.06
Average Without NLT Mat:	**3.94**	**1.08**
Green, Scrailed NLT Mat	4.20	1.07
Average With NLT Mat:	**3.96**	**1.09**

Table 4.11. Costs associated with labor and materials, energy usage, and final disposal of NLT crane mats

Material and Labor Costs			
Cost Item	**Price ($)**	**Quantity/ Mat**	**Total ($)/ Mat**
1.25 in. x 7.5 in. x 8 ft Piece of Lumber	4.68	72	336.96
15° Wire Coil Nail	0.013	1,440	18.72
R4 Multipurpose Framing Screw	0.10	336	33.60
20° Jumbo Plastic Strip Scrail	0.11	528	56.08
4 ft Threaded Rod	2.69	4	10.76
Nut and Fender Washer	0.35	8	2.80
Labor Rate for Two People	35.00/hr	3 hr	105.00
Overhead Cost	30.00/hr	3 hr	90.00
Energy Costs			
Cost Item	**Energy Usage (wt)**	**Time (hrs)/ Mat**	**Total ($)/ Mat**
Electricity to Cut Each Board to Size Using a Table Saw	1,000	0.10	0.01
Electricity to Install Each Nail Using a Nail Gun	1,650	1.32	0.11
Electricity to Install Each Screw Using a Corded Drill	300	0.14	0.01
Electricity to Install Each Scrail Using a Nail Gun	1,650	0.46	0.04
Electricity to Drill Holes for Threaded Rods Using a Corded Drill	300	0.02	0.01
Final Disposal Costs			
Cost Item	**Price ($)**	**Quantity/ Mat**	**Total ($)/ Mat**
Transportation via Flatbed Truck	3.14/mi	100 mi	314.00
Landfill	48.40/ton	0.75 ton	36.30
Total Crane Mat Cost ($)	**Nailed NLT Mat**		**914.66**
	Screwed NLT Mat		**929.44**
	Scrailed NLT Mat		**953.95**

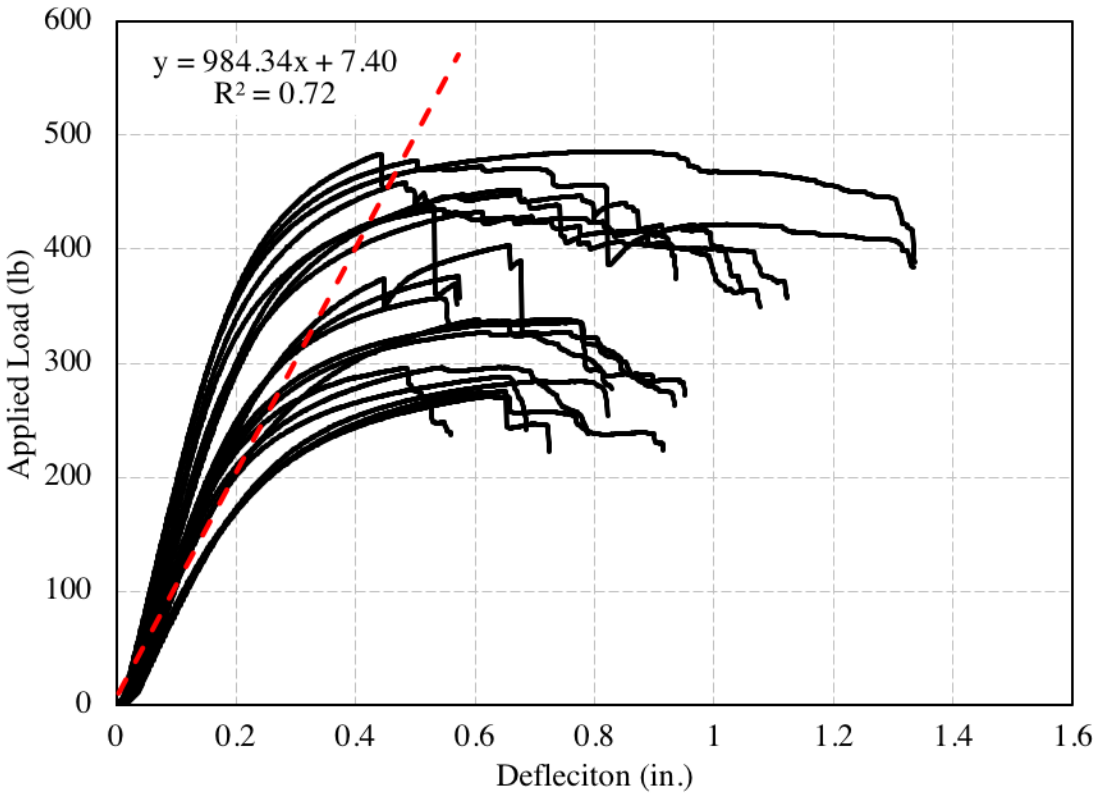

Figure 4.1. Applied load vs. deflection curves and associated linear trendline of the MOE specimens tested at the NRRI

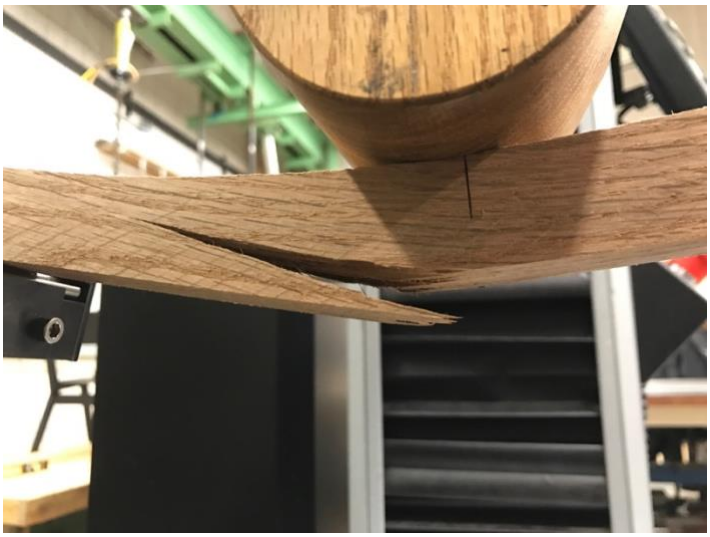

Figure 4.2. Profile view of a typical cross grain tension failure in the MOE specimens

Figure 4.3. View of the tension surface following a typical splintering tension failure in the MOE specimens

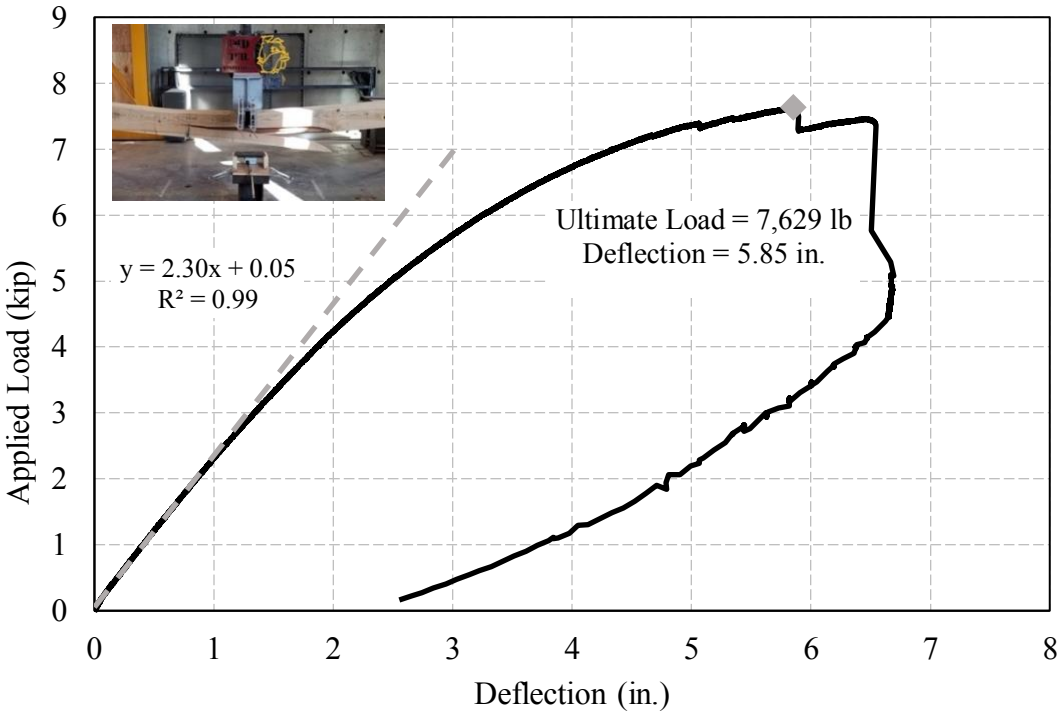

Figure 4.4. Applied load vs. deflection curve for the Solid Timber (1) specimen

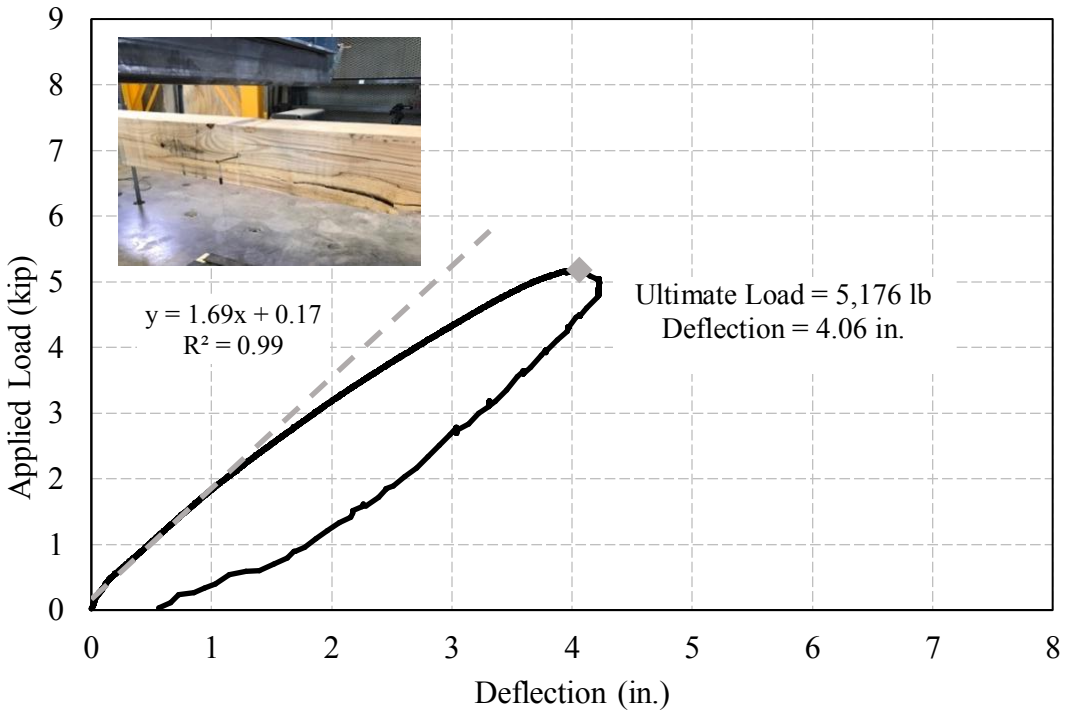

Figure 4.5. Applied load vs. deflection curve for the Solid Timber (2) specimen

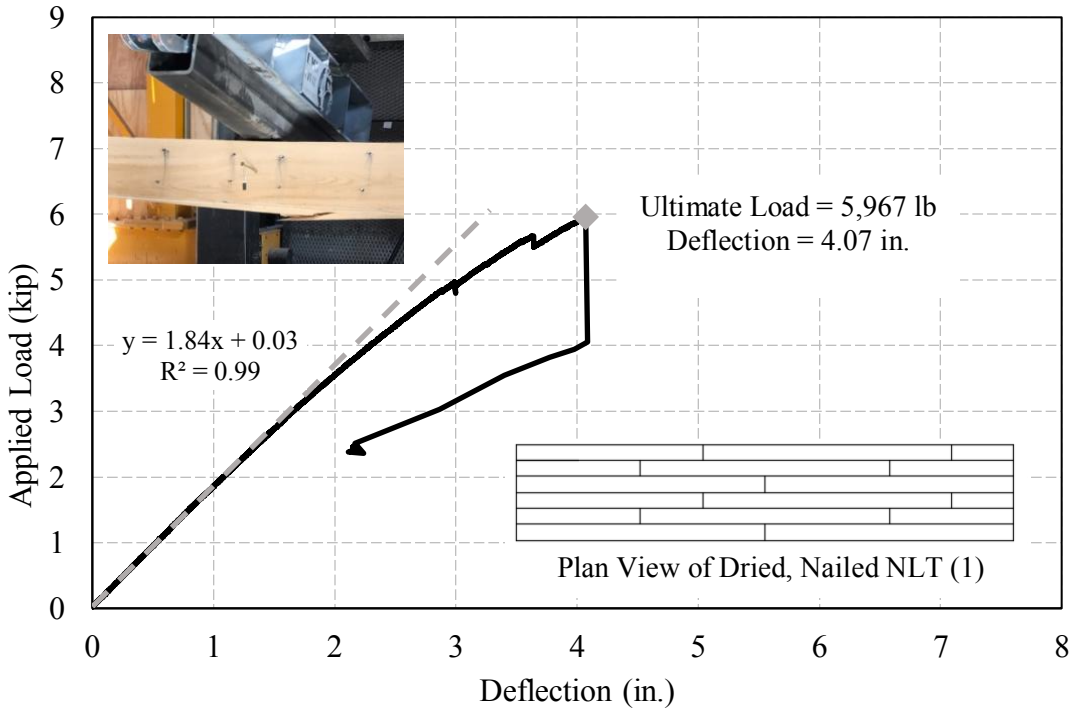

Figure 4.6. Applied load vs. deflection curve for the Dried, Nailed NLT (1) specimen

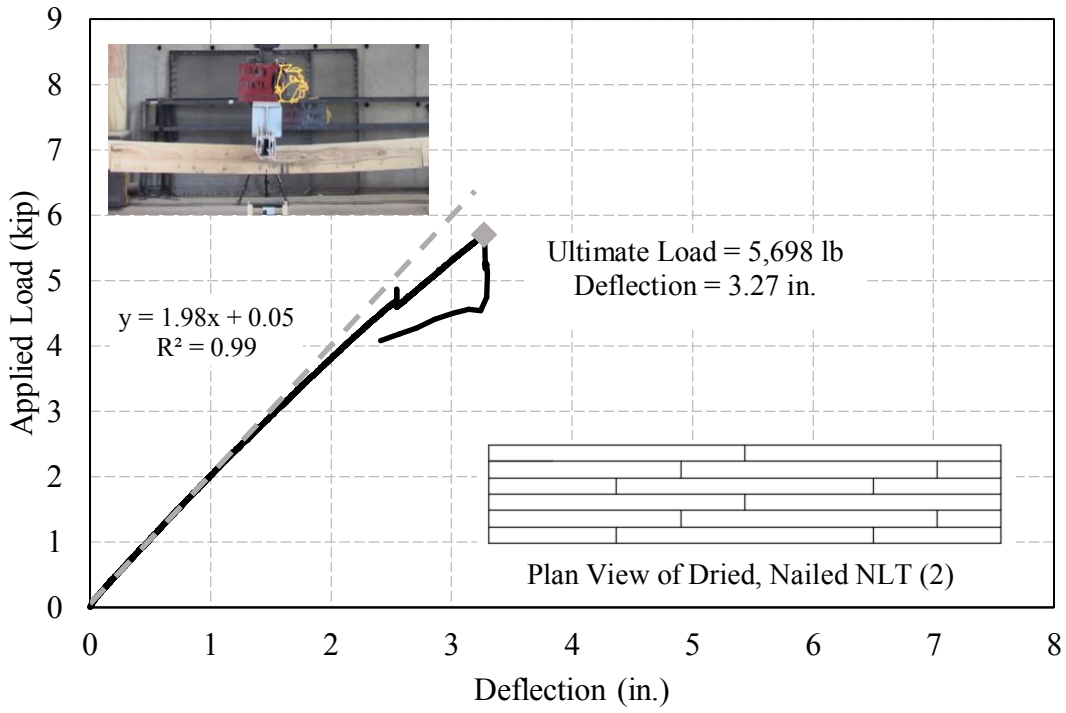

Figure 4.7. Applied load vs. deflection curve for the Dried, Nailed NLT (2) specimen

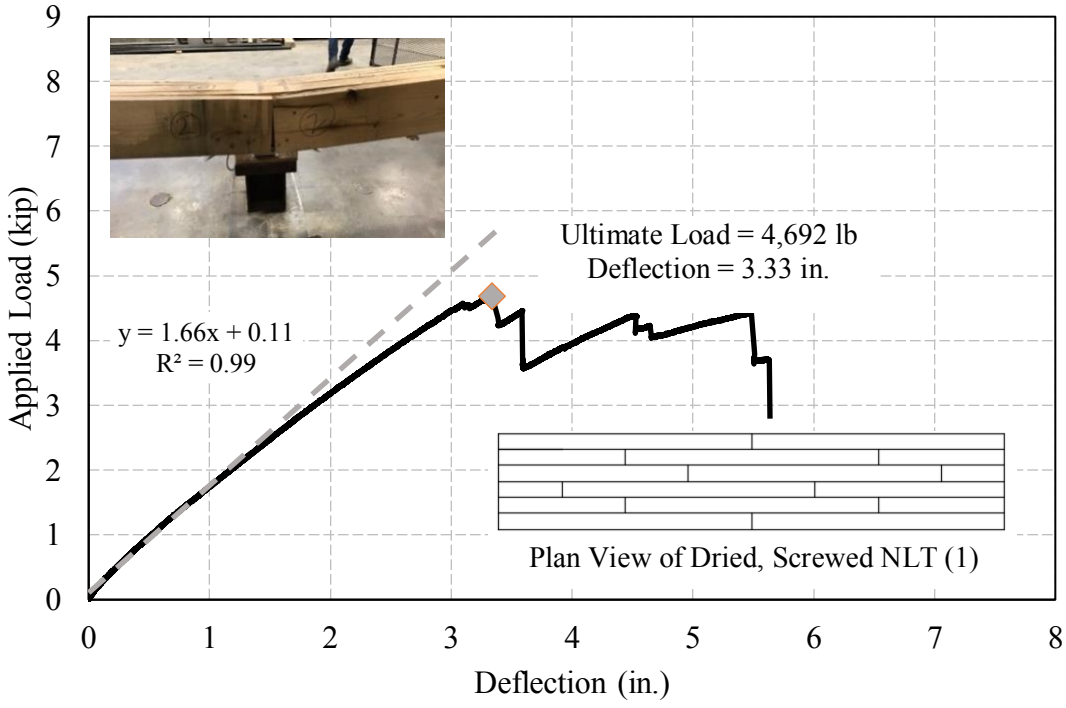

Figure 4.8. Applied load vs. deflection curve for the Dried, Screwed NLT (1) specimen

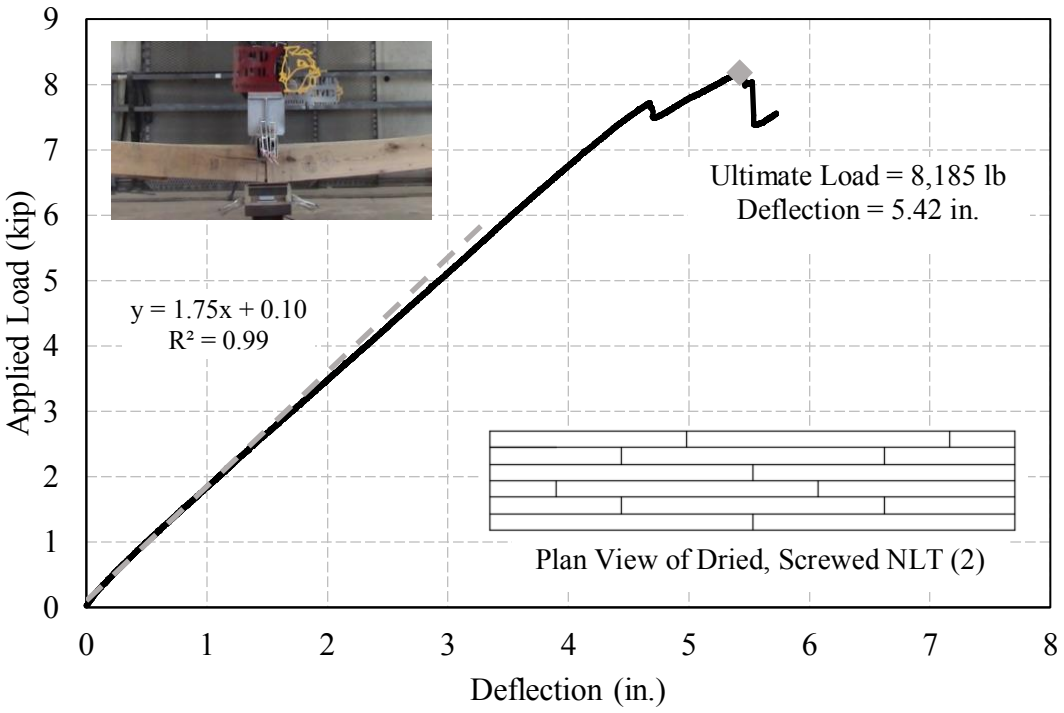

Figure 4.9. Applied load vs. deflection curve for the Dried, Screwed NLT (2) specimen

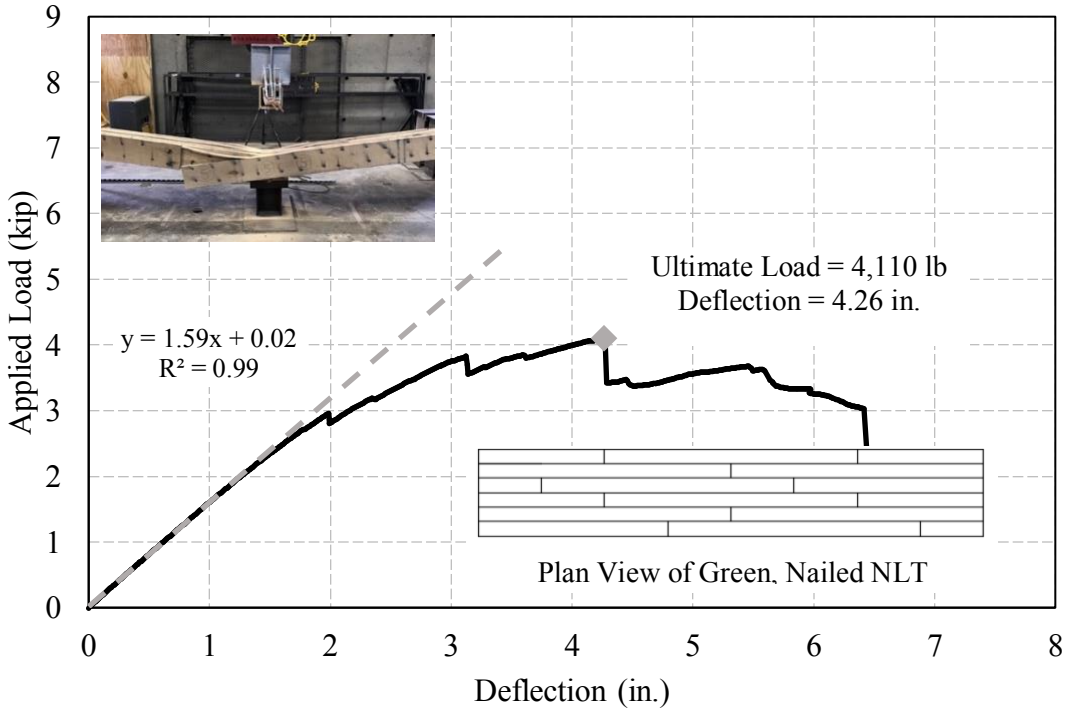

Figure 4.10. Applied load vs. deflection curve for the Green, Nailed NLT specimen

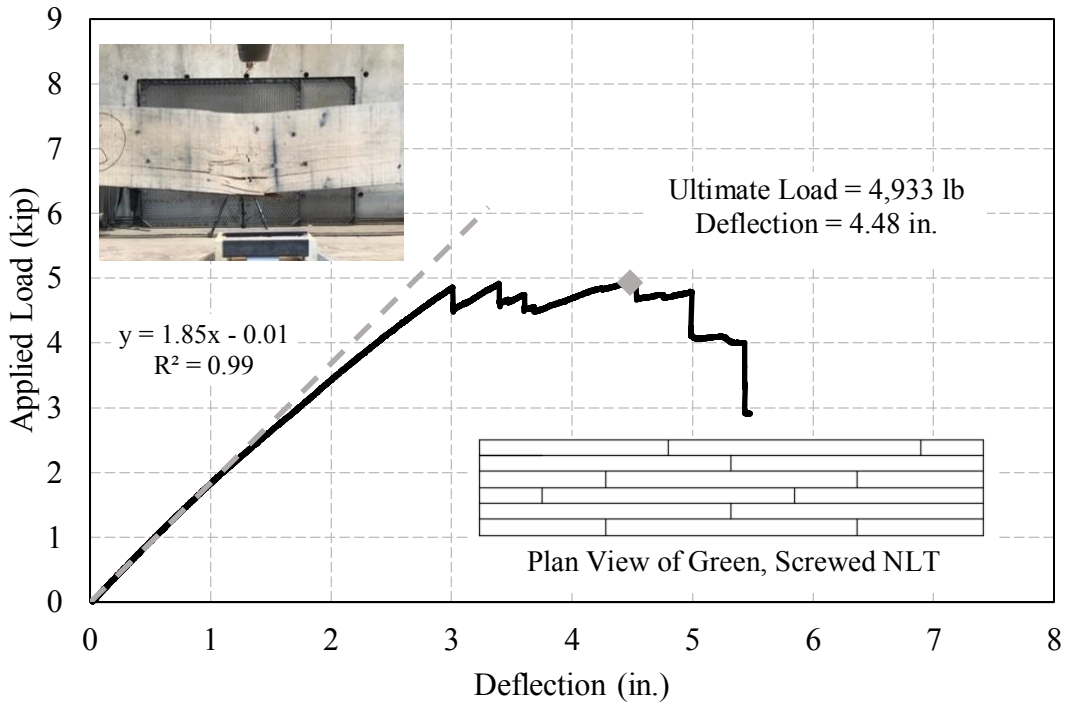

Figure 4.11. Applied load vs. deflection curve for the Green, Screwed NLT specimen

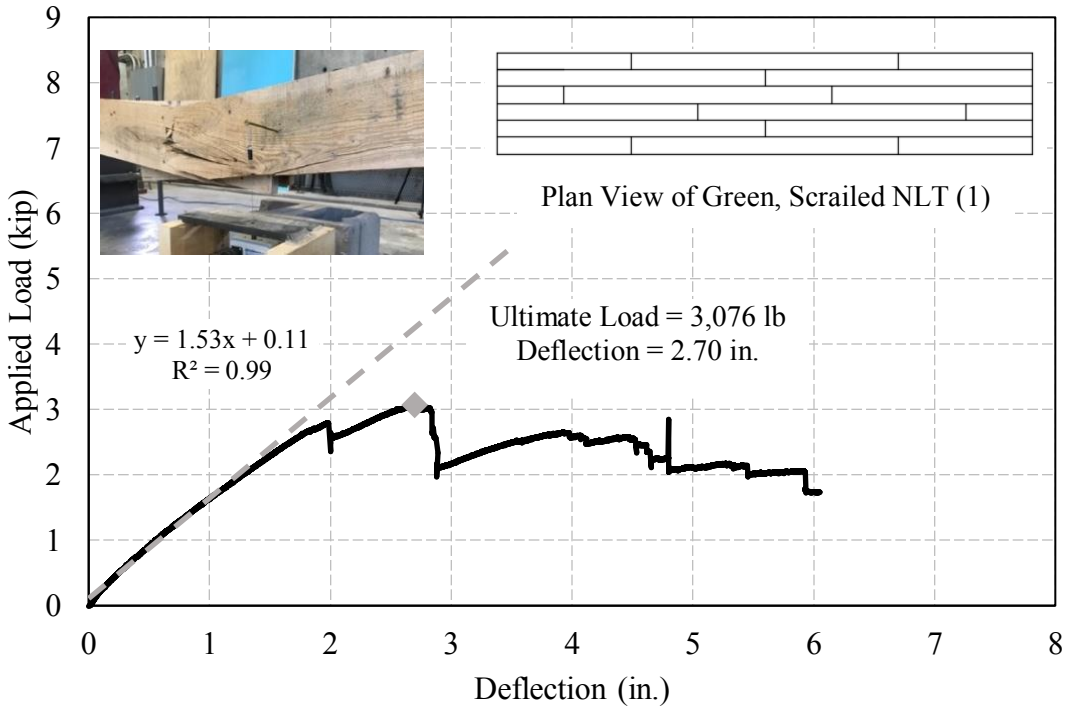

Figure 4.12. Applied load vs. deflection curve for the Green, Scrailed NLT (1) specimen

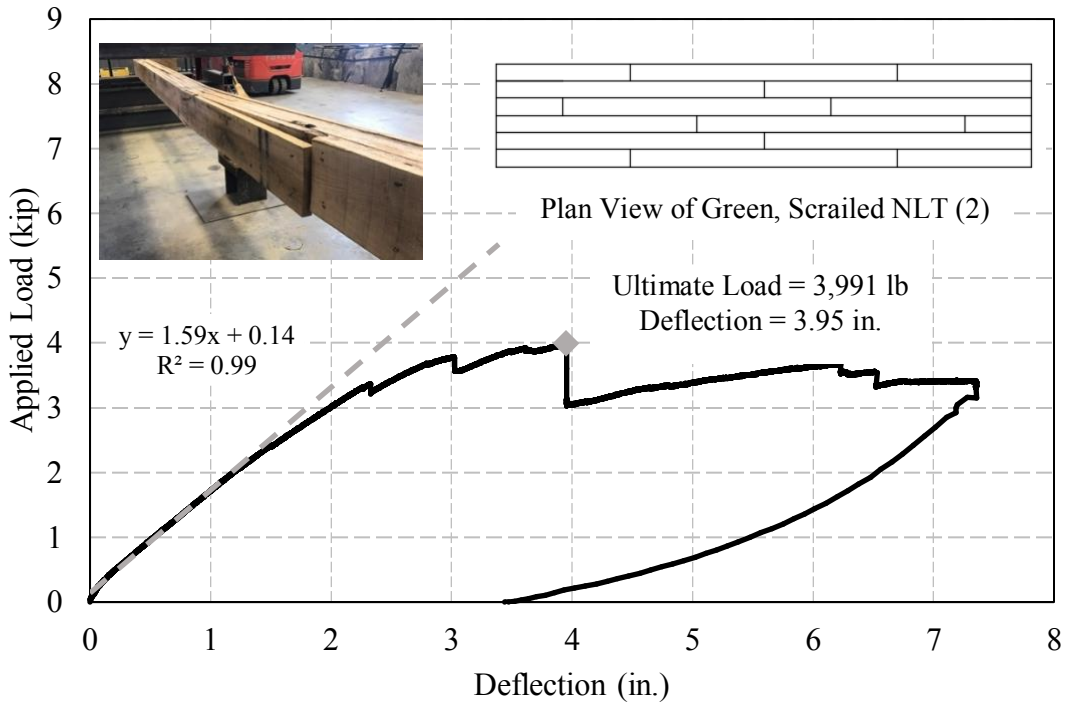

Figure 4.13. Applied load vs. deflection curve for the Green, Scrailed NLT (2) specimen

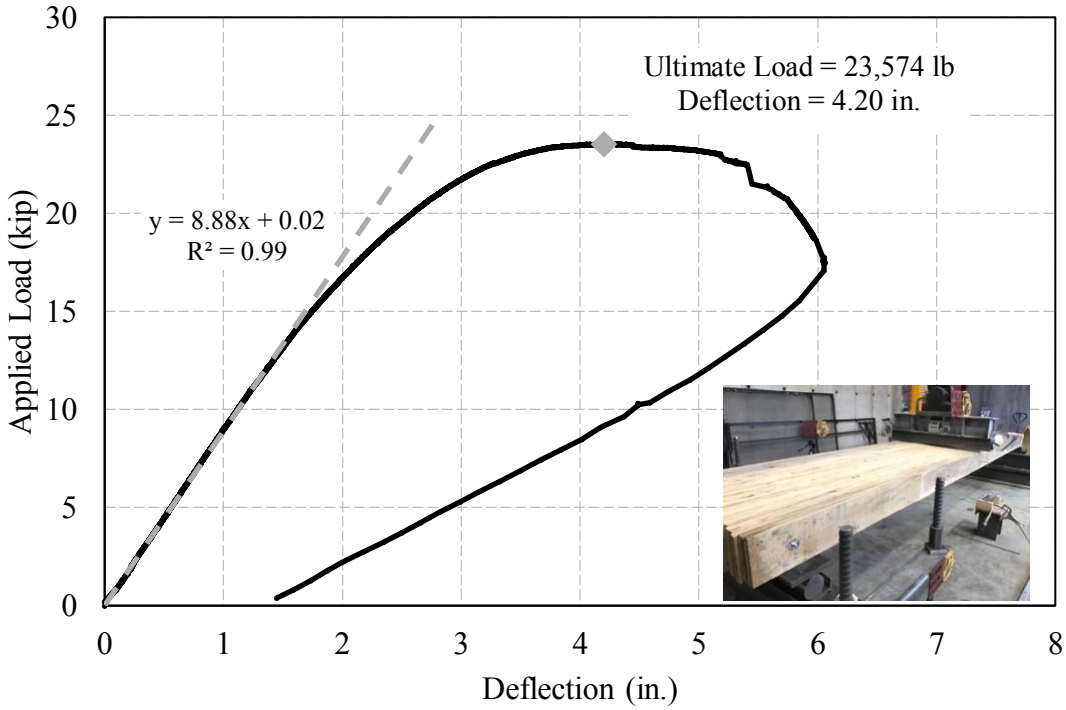

Figure 4.14. Applied load vs. deflection curve for the Green, Scrailed NLT Mat specimen

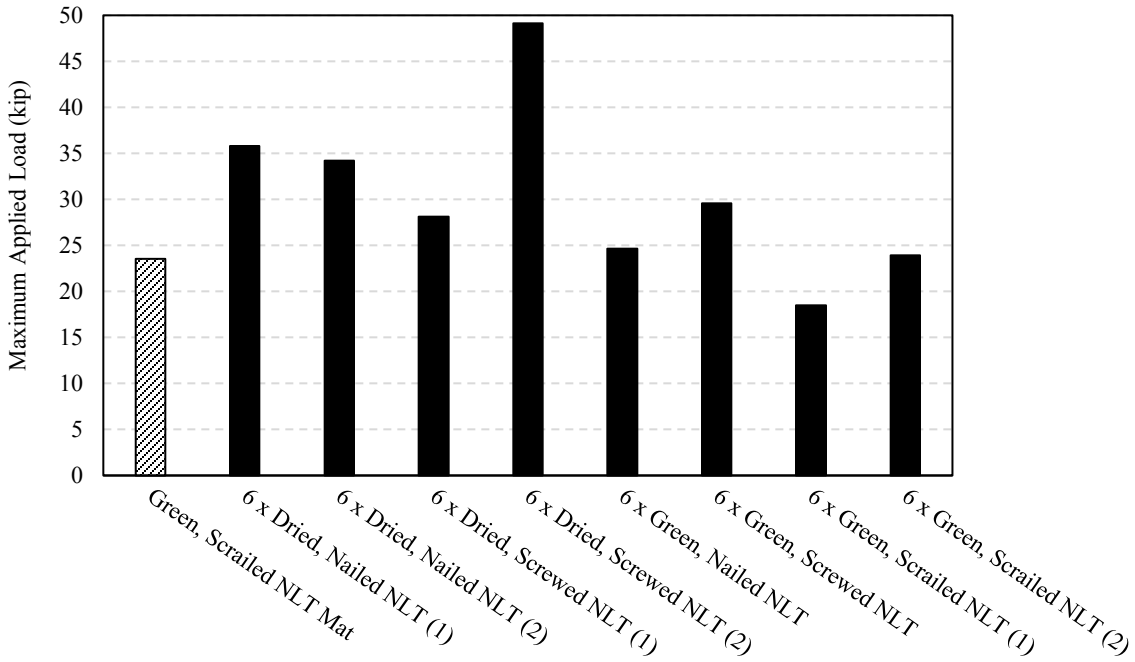

Figure 4.15. Green, Scrailed NLT Mat maximum applied load compared to six times the maximum applied load exhibited by each individual NLT specimen

Figure 4.16. Cross grain tension failure in the Solid Timber (1) specimen

Figure 4.17. Cross grain tension failure in the Solid Timber (2) specimen originating from a knot

Figure 4.18. Tension failure of the interior laminations in the Dried, Nailed NLT (1) specimen

Figure 4.19. Typical compression failure at the butt joint in the Dried, Screwed NLT (1) specimen

Figure 4.20. Nails pulled through the exterior lamination near a butt joint resulting in connection failure between the laminations in the Green, Nailed NLT specimen

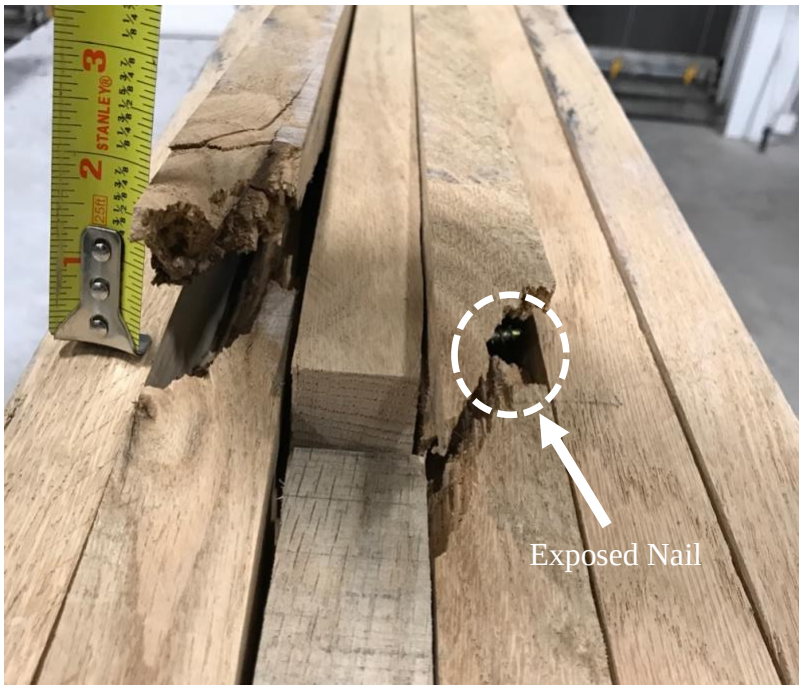

Figure 4.21. Cross grain tension failure in two of the interior laminations that exposed nails in the Dried, Screwed NLT (1) specimen

Figure 4.22. Typical crack at the butt joint that extended parallel to the grain of the wood toward the load

Figure 4.23. Splintering tension and compression failures observed in the Green, Screwed NLT specimen

Figure 4.24. Cracks propagating toward a knot in the exterior lamination beneath the applied load

Figure 4.25. Tension failure in the exterior lamination of the Green, Scrailed NLT Mat

CHAPTER 5. SUMMARY, CONCLUSIONS AND RECOMMENDATIONS

5.1 Summary

This research was part of a project conducted in collaboration with Savanna Pallets, Inc. of Cloquet, MN and the University of Minnesota Duluth Natural Resources Research Institute. As part of this project, two solid 7.5 in. wide x 7.5 in. deep x 16 ft long timber beams, eight 7 in. wide x 8 in. deep x 16 ft long NLT beams, and one 4 ft wide x 8 in. deep x 16 ft long NLT mat were fabricated at Savanna Pallets, Inc. and the UMD structures laboratory. This project had three specific goals. The first was to evaluate if NLT panels can be effectively manufactured using underutilized, small diameter, local wood species in collaboration with Savanna Pallets, Inc. The second goal was to experimentally determine the flexural strength of the different NLT crane mat designs and compare the results to current design recommendations for structural applications as there is currently no such performance standards for crane mats. The third goal was to determine the cost of a 4 ft wide x 8 in. deep x 16 ft long crane mat fastened with nails, screws, or scrails and if production would be economically feasible.

The NLT specimens were constructed using a rough cut northern red oak lumber and the individual laminations were fastened together using either screws, nails, or scrails. Each specimen was evaluated using a three point bending test configuration to determine the maximum applied point load, the deflection at the maximum applied point load, and the MOE. Maximum applied point load, deflection, and MOE calculations were performed using the IBC (2018) and the NLT Design Guide (2017). Final comparisons were used to determine if the Code provisions that are used for structural applications produce conservative results for this type of NLT construction. In addition to the flexural testing performed at UMD, 1 in. wide x 1 in. deep x 16 in. long specimens were cut from the northern red oak used in this project and 20 samples were tested at the NRRI to determine the stiffness of the lumber. Measured values for MOE were compared among specimens and to theoretical predictions calculated using the NLT Design Guide (2018).

5.2 Conclusions

The following conclusions were drawn based on the results and observations of the tests and cost analysis performed within this project:

1. The solid timber specimens used as a baseline for testing exhibited a higher average maximum applied point load that was 26% greater than the NLT beam specimens (calculated by dividing the average maximum applied point load for the solid timber specimens by the average maximum applied point loads exhibited by the NLT beam specimens in Table 4.2. and converting to a percentage). However, the Dried, Screwed NLT (2) specimen displayed a higher flexural strength than either of the two solid timbers.
2. NLT specimens that were constructed using the #12 x 5-5/8" R4^{TM} Multi-Purpose Framing Screws exhibited the highest flexural strength. The average maximum applied point load for the screwed NLT specimens was 13% greater than the average maximum applied point load exhibited by the nailed NLT specimens (calculated by dividing the average maximum applied point load for the screwed NLT specimens by the average maximum applied point load for the nailed NLT specimens in Table 4.4 and converting to a percentage). The NLT beam specimens constructed with 20° Plastic Strip Jumbo Scrails exhibited the lowest flexural strength, which was 33% lower than the average maximum applied point load for the nailed NLT specimens (calculated by dividing the average maximum applied point load for the scrailed NLT specimens by the average maximum applied point load exhibited by the nailed specimens in Table 4.4 and converting to a percentage).
3. Using a random lamination layup design for NLT specimens resulted in a measured flexural strength that was approximately 1.5 times greater than the symmetric layup design (calculated by dividing the average maximum applied point load for the NLT specimens constructed with the random lamination layup by the average maximum applied point load for the symmetric layup NLT specimens in Table 4.4). All of the specimens constructed with a symmetric layup were fastened together using only the 20° Plastic Strip Jumbo Scrails, whereas the specimens constructed with a random layup were fastened together with either the 15° Wire Coil Nails or the #12 x 5-5/8" R4^{TM} Multi-Purpose Framing Screws.

4. The Green, Scrailed NLT Mat, which was constructed of six of the Green, Scrailed NLT beams, exhibited a flexural strength that was 11% greater than the average strength of the individual Green, Scrailed NLT beams multiplied by six (calculated by dividing the maximum applied point load exhibited by the Green, Scrailed NLT Mat by six times the average maximum applied point load for the Green, Scrailed NLT beam specimens in Table 4.4 and converting to a percentage).
5. In general, the NLT specimens exhibited cross grain and splintering tension failures in laminations that were continuous underneath the applied load. Compression failures frequently occurred at butt joints located 0 to 2 ft from the applied load.
6. The MOE of the northern red oak determined through testing in accordance with ASTM D198 (2015) was less than the MOE obtained from data collected during testing of all of the NLT specimens. This indicated that the NLT beams were more stiff compared to the northern red oak lumber.
7. The Code predictions for flexural strength and MOE were conservative for all of the NLT specimens, and the theoretical deflections were much less than those measured during testing. The IBC (2018) based method provided results that were approximately 11% lower than the experimental maximum applied point loads (calculated by dividing the average maximum applied point load for the IBC method by the experimental average maximum applied point load in Table 4.8 and converting to a percentage). The NLT Design Guide (2017) method yielded an average maximum applied point load that was approximately 74% lower than the experimental average maximum applied point load (calculated by dividing the average maximum applied point load for the NLT Design Guide method by the experimental average maximum applied point load in Table 4.8 and converting to a percentage).
8. It was economically feasible to manufacture NLT crane mats constructed with 15° Wire Coil Nails, #12 x 5 5/8" R4™ Multi-Purpose Framing Screws, and 20° Plastic Strip Jumbo Scrails comparing production costs of NLT mats to quoted purchase costs of solid timber mats. However, it was not practical to landfill a large volume of mats or chip and dispose NLT crane mats that contain metal fasteners that could not be easily removed after use.

5.3 Recommendations for Future Research and use of NLT Crane Mats

The research and results pertaining to this thesis were based on two solid timber and nine NLT specimens designed using a variety of construction methods. Additional research with a larger sample size for each unique design would help to better understand the flexural behavior of NLT crane mats constructed with rough cut northern red oak lumber. Further investigation is also needed to accurately quantify the properties of lumber used in this research as the test specimens were chosen based on the controlling party's desires. Once the flexural behavior of the lumber is more fully understood, the performance of the different fastener types and spacing patterns used to construct NLT specimens with continuous laminations should be evaluated. The research presented in this thesis did not use the same spacing and number of fasteners in each NLT specimen. Therefore, further research should be done to determine which fastener provides the strongest connection between laminations and its contribution to the flexural strength. Additionally, the effect of butt joint locations should be investigated but would require a larger sample size and consistent designs. Although random butt joint locations may be more feasible for mass production of NLT crane mats, further research is needed to determine the locations that would be most economical without compromising the flexural strength of the NLT.

From experimental and theoretical test results within the scope of this research project, design of butt-jointed NLT crane mats with low grade lumber and a variety of fasteners was found to be practical. However, NLT crane mats with metal fasteners cannot be chipped for reuse and producing them in large volumes would result in impractical disposal methods and costs. Further research is recommended to determine alternative methods of disassembly and disposal of NLT crane mats.

REFERENCES

AITC 112-93. (1993). "Standard for Tongue and Groove Heavy Timber Roof Decking." American Institute for Timber Construction (AITC), Englewood, CO.

Alberta Rig Mats (2018). "Alberta Rig Mats Features." New Sarepta, AB.

American Institute of Steel Construction (AISC). (2011). Steel Construction Manual (14th Edition), Chicago, IL.

American Wood Council (2014). NDS National Design Specification for Wood Construction. Leesburg, VA: American Wood Council.

ANSI/PRG 320 - 2012. (2012). "Standard for Performance-Rated Cross-Laminated Timber." American National Standards Institute (ANSI), New York, NY.

ASTM D143 – 14. (2014). "Standard Test Methods for Small Clear Specimens of Timber." American Society for Testing and Materials (ASTM), West Conshohocken, PA.

ASTM D198 – 76. (1976). "Standard Test Methods of Static Tests of Lumber in Structural Sizes." American Society for Testing and Materials (ASTM), West Conshohocken, PA.

ASTM D198 – 84. (1984). "Standard Test Methods of Static Tests of Lumber in Structural Sizes." American Society for Testing and Materials (ASTM), West Conshohocken, PA.

ASTM D198 – 92. (1992). "Standard Test Methods of Static Tests of Lumber in Structural Sizes." American Society for Testing and Materials (ASTM), West Conshohocken, PA.

ASTM D198 – 15. (2015). "Standard Test Methods of Static Tests of Lumber in Structural Sizes." American Society for Testing and Materials (ASTM), West Conshohocken, PA.

Beck Fastener Group. (2018). "Plastic Strip Jumbo Scrail Applications." Mauerkirchen, AU.

Bohnhoff, D., Moody, R., Verill, S., Shirek, L., (1991), "Bending Properties of Reinforced and Unreinforced Spliced Nail-Laminated Posts." United States Department of Agriculture, Madison, WI.

Cross-Laminated Timber (CLT) Handbook. (2013). FP Innovations and Binational Softwood Lumber Council, Surrey, BC.

Currier, R.A., (1955), "Strength and Stiffness of Random-length End-and Center-matched 2- by 6-inch Douglas Fir Decking." Oregon Forest Products Laboratory, Corvallis, OR.

DAT Solutions, LLC, (2018). "DAT Trendlines." Beaverton, OR.

Haller, P., (2000), "Experimental and numerical study of nailed laminated timber elements for in-plane and transverse loading," in World Conference on Timber Engineering, Whistler BC, 2000.

International Code Council. (2015). "Design of Wood Structures ASD/LRFD (7th Edition)." Country Club Hills, IL: ICC.

International Code Council. (2018). "International Building Code." Country Club Hills, IL: ICC.

Koch, L. (2018). Personal Email Communication. October 8, Duluth, MN.

Koen, K. (2018). Personal Email Communication. May 1 through November 12, Duluth, MN.

Kraemer, V., Blass, H.J., (2001). "Load Carrying Capacity of Nail-Laminated Timber Under Concentrated Loads." Karlsruhe, DE.

Kraemer, V., (2004). "Load Carrying Capacity of Nail-Laminated Timber loaded perpendicular to its plane." Structural Building Components Associated, June 2004.

Mathcad Prime (Version 1.0) [Computer software]. (2011). PTC.

Matrax, Inc. (2018). "Matrax Temporary Road Mats." Columbia, MD.

Minnesota Power. (2009). "Minnesota Power Electric Rate Book." Duluth, MN.

Nail-Laminated Timber U.S. Design and Construction Guide v1.0. (2017). Binational Softwood Lumber Council, Surrey, BC.

Northern Mat & Bridge. (2018). "Steel Framed Mat Specifications." Steel Framed Mats/Rig Mats, Clairmont, AB.

Payson City Corporation. (2018). "Energy-Use Charts." Payson City, UT.

Quality Mat Company. (2018). "Crane Mat Uses." Beaumont, TX.

Rig Mats of America, Inc. (2018). "Crane Mats." Billings, MT.

Spartan Mat, LLC. (2018). "Protecting Equipment, Workers, and the Environment." Crane Mats, Portland, OR.

Sterling. (2018). “Stability and Support for The Heaviest Equipment.” Crane Mats, Chicago, IL.

StrucutreCraft Builders, Inc. (2018). “Nail Laminated Timber – NLT.” Abbotsford, BC.

TerraPro, Inc. (2018). “Access Matting.” Sherwood Park, AB.

Thompson, J., (2017), “Landfill Waste Costs Continued to Rise in 2016.” Solid Waste Environmental Excellence Protocol (SWEEP).

Tufftrak Ground Protection Solutions. (2018). “Innovative Mat Design.” Advantages and Technology, Broomfield, CO.

Williams, G, Bohnhoff, D., Moody, R., (1994). “Bending Properties of Four-Layer Nail-laminated Posts.” United States Department of Agriculture, Madison, WI.

Winistorfer, S., Moody, W., Cramer, C., (1987). “Bending Performance of Spliced, Nailed-Laminated Posts.” American Society of Agriculture and Biological Engineers (ASABE) Vol. 30, St. Joseph, MI.

APPENDIX A. STRING POT INSTALLATION AND SETUP

This appendix describes the installation and setup of the Unimeasure P510 Series string pot that was used to measure deflection during testing at the UMD structures laboratory. The following steps describe how to install the string pot and make the proper adjustments to the National Instruments (NI) computer system for compatibility.

1. Remove the string pot and cable from any packaging, then locate red, blue, black and white wires protruding from the end of the cable shown in Figure A.1.
2. The red, blue, black, and white wires will likely need to be extended, which can be achieved by splicing the wires with ordinary wire. The blue and white wires were spliced with spare red and black wires, respectively, but are labeled with the correct color for the installation as shown in Figure A.2.
3. Obtain a DB9 connector and locate pins 1 and 2 as shown in Figure A.3.
4. Solder the black wire to pin 1 and the red wire to pin 2 as shown in Figure A.4.
5. Place the DB9 connector and wires in the provided casing as shown in Figure A.5 and install the cover using a small screw driver. The final wire and connector assembly is shown in Figure A.6.
6. Insert the DB9 connector in one of the excitation plugins on the back of the SC6000 Auxiliary Excitation I/O Module as shown in Figure A.7 (note that any of the eight plugins will work as the string pot can accept both 15VDC and 24VDC excitation).
7. Locate the preferred NI SCXI-1327 high-voltage attenuator terminal block on the back of the NI SCXI-1121 computer system (one that is open or will not be in use during testing). Then, loosen the screws at the top and bottom of the chosen terminal block and carefully remove it from the NI SCXI-1121 module as shown in Figure A.8.
8. Gently place the terminal block on a flat surface then completely remove the two screws on the side of the terminal block as shown in Figure A.9 and remove the cover.
9. Loosen the two screws holding any existing wires in place as shown in Figure A.10.
10. Locate an open channel that will be used for excitation of the string pot and loosen the screws on the positive and negative terminals as shown in Figure A.11. Channel 2 was chosen for the installation shown in this appendix.
11. Insert the wires through opening on the terminal block that was previously loosened. Then, insert the blue and white wires into the positive and negative terminals,

respectively, and tighten the positive and negative terminal screws so the wires and snug as shown in Figure A.12.

12. Tighten the screws that were previously loosened in step 9 to secure the opening on the terminal block.
13. Bypass the attenuator on the selected channel by moving the corresponding switch positions from 100:1 to 1:1 as shown in Figure A.13. This is also described on page 5 of the SCXI-1327 High-Voltage Attenuator Terminal Block Installation Guide.
14. Replace the cover and two screws on the side of the terminal block that were removed in step 8 and verify that the wires are still connected by gently tugging on them from the outside of the terminal block.
15. Loosen the screws at the top and bottom of the NI SCXI-1121 module as shown in Figure A.14 and carefully remove it from the rest of the computer.
16. Remove the three screws from the cover plate on the back on the module as shown in Figure A.15 and gently slide the circuit board out of the metal casing as shown in Figure A.16.
17. Locate the gain jumpers on the circuit board associated with the selected excitation input channel as shown in Figure A.17. A list of the channels and their corresponding gain jumpers can be found on page 2-9 of the SCXI-1121 User Manual. As channel 2 was selected for the installation described in this appendix, the first gain jumper is W29 and the second gain jumper is W30. A detailed layout of the gain jumper locations is shown on page 2-2 of the SCXI-1121 User Manual.
18. Move the first gain jumper (W29) to position D and the second gain jumper (W30) to position A as shown in Figure A.18 (note that the factory setting for the first gain jumper is position A and the second gain jumper is position D).
19. Once the gain jumpers have been moved to the appropriate positions, insert the circuit board back in to the metal casing.
20. Replace the cover plate and the three screws that were removed from the NI SCXI-1121 module in step 16.
21. Insert the NI SCXI-1121 module back into the NI computer system and tighten the screws at the top and bottom of the module as shown in Figure A.19.

22. Insert the SCXI-1327 high-voltage attenuator terminal block into the NI SCXI-1121 module and tighten the screws at the top and bottom of the terminal block as shown in Figure A.20.
23. Connect the opposite end of the cable to the Unimeasure P510 Series string pot as shown in Figure A.21.
24. Start the computer system and open the Shore Western startup application.
25. Select “Portal Frame” from the panel list and select the “Main Panel” from the program list.
26. Select the channel being used in the bottom left corner of the screen as seen in Figure A.22. If the desired channel is not listed, it can be added by clicking on the “Select Channels” option and adding it from the available channels. The channel name corresponding to the installation shown in this appendix is “1121 Mod3 ai2”. This references the third NI SCXI-1121 module as “Mod3” and excitation channel 2 as “ai2”.
27. Once the correct channel has been selected, a voltage output is displayed on the screen directly above the list of channels as shown in Figure A.23.
28. Extend the wire on the string pot until it has reached approximately half of its entire stroke.
29. With the wire extended, use a small screwdriver to turn the dial labeled “zero” on the side of the string pot as shown in Figure A.24. Continue turning the dial until the voltage output reaches approximately zero volts.
30. Use the small screwdriver to turn the dial labeled “span” on the side of the string pot until the voltage output extends across the entire stroke of the wire. In order to ensure that the voltage will change throughout the entire stroke of the wire, the “span” will likely need to be adjusted to its maximum setting.
31. After verifying that the voltage output changes across the entire stroke of the wire, calibrate the string pot using a calipers or ruler.

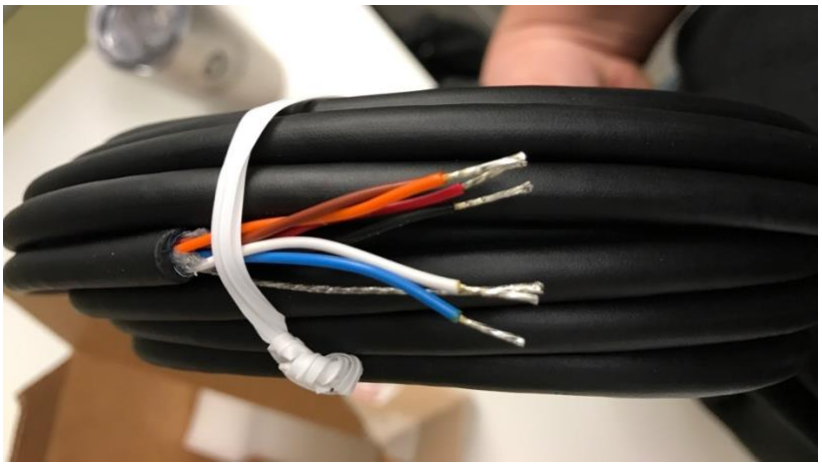

Figure A.1. Red, blue, black, and white wires protruding from the string pot cable

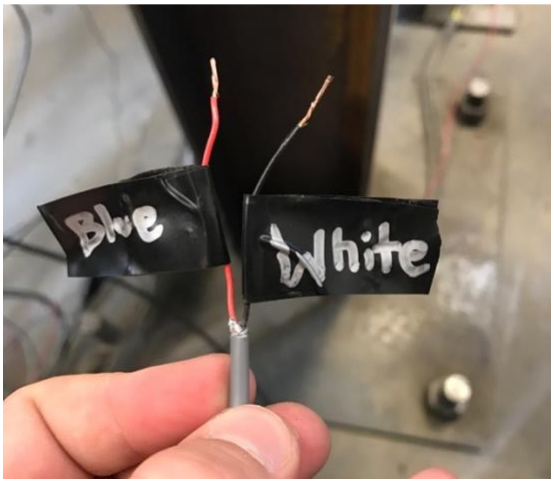

Figure A.2. Blue and white wires spliced with spare black and red ordinary wire

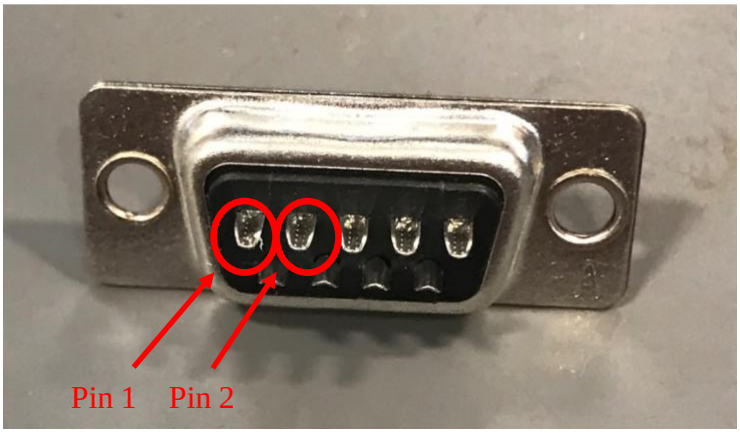

Figure A.3. Location of pins 1 and 2 on the DB9 connector

Figure A.4. Black and red wires respectively soldered to pins 1 and 2

Figure A.5. DB9 connector and wires placed in the provided casing

Figure A.6. Final wire and connector assembly

Figure A.7. DB9 connector being plugged into the SC6000 Auxiliary Excitation I/O Module

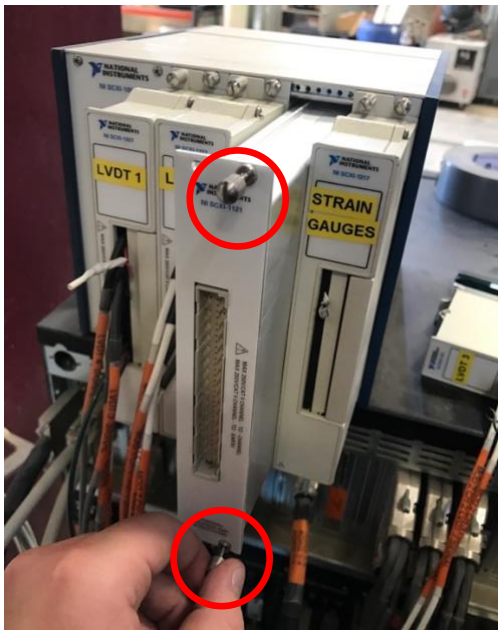

Figure A.8. Loosen the two screws at the top and bottom of the NI SCXI-1327 high-voltage attenuator terminal block

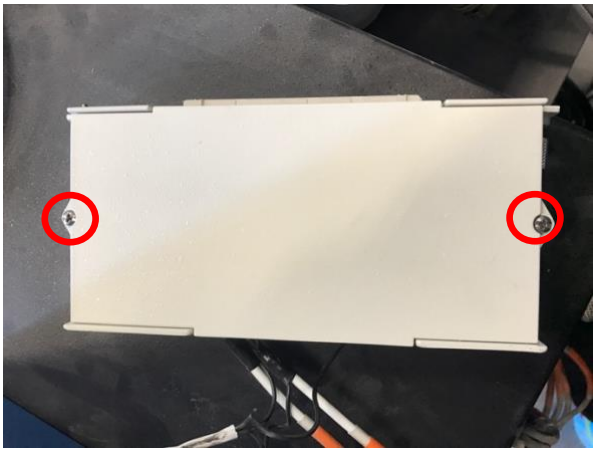

Figure A.9. Remove the two screws and cover from the NI SCXI-1327 high-voltage attenuator terminal block

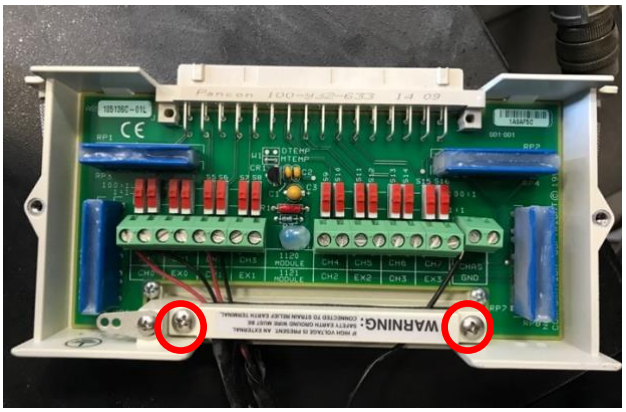

Figure A.10. Loosen the two screws holding any existing wires in place

Figure A.11. Loosen screws at positive and negative terminal for the selected channel

Figure A.12. Insert the blue and white wires into the positive and negative terminals, respectively, and tighten the terminal screws

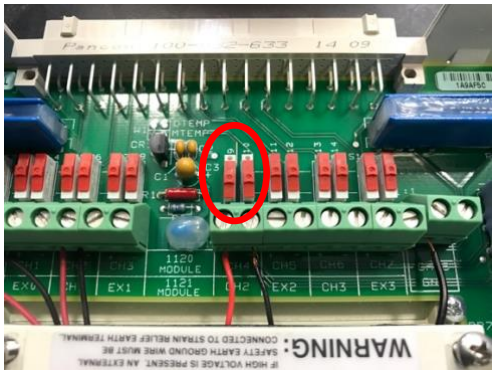

Figure A.13. Bypass the attenuator on the selected channel by moving the switch positions down from 100:1 to 1:1

Figure A.14. Loosen the two screws on the NI SCXI-1121 module and carefully remove

Figure A.15. Remove the three screws and cover plate from the back of the NI SCXI-1121 module

Figure A.16. Slide the circuit board out from the casing

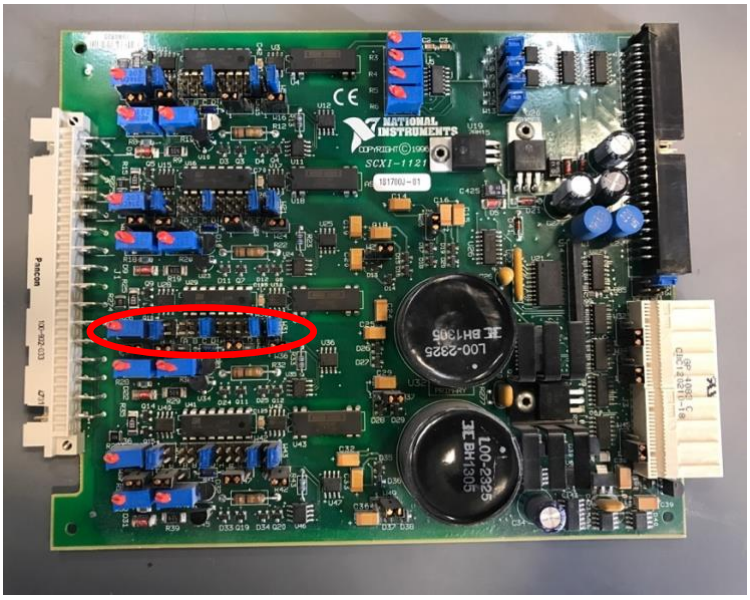

Figure A.17. Locate the gain jumpers for the selected channel

Figure A.18. Move the first gain jumper (W29) to position D and the second gain jumper (W30) to position A

Figure A.19. Replace the NI SCXI-1121 module

Figure A.20. Replace the SCXI-1327 high-voltage attenuator terminal block and tighten the two screws

Figure A.21. Connect string pot and cable

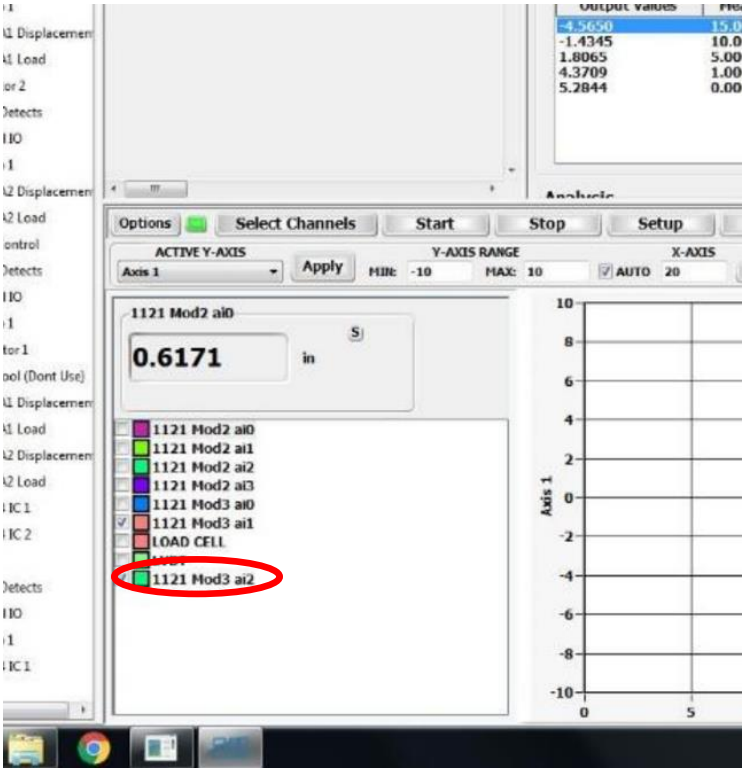

Figure A.22. Click on the selected channel in the bottom left corner of the screen

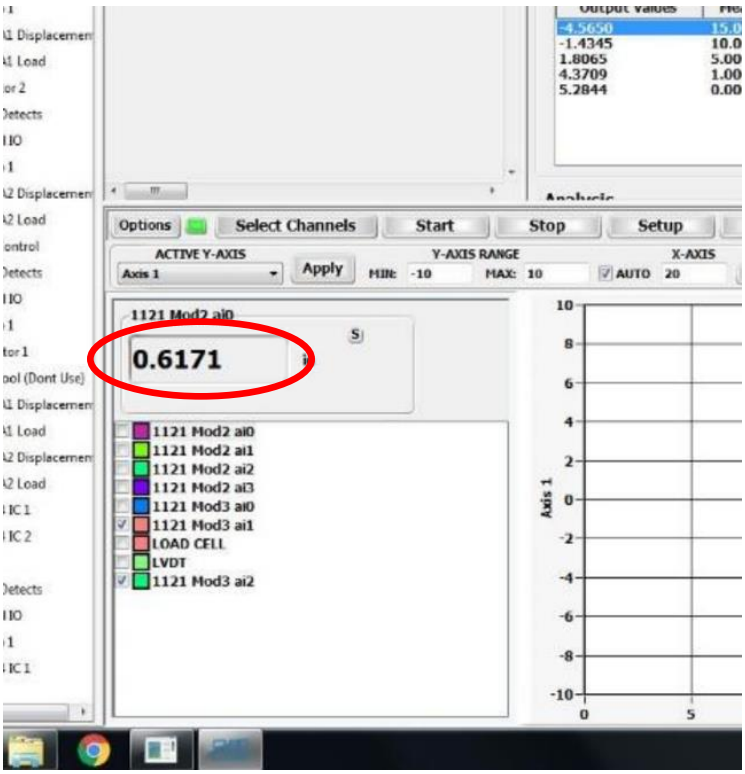

Figure A.23. Voltage output is located above the available channels

Figure A.24. Adjust the "zero" dial until there is a voltage output of zero when the string pot wire is extended to approximately half of its entire stroke

APPENDIX B. FLEXURAL STRENGTH CALCULATIONS

All calculations shown in this appendix were made using Mathcad Prime (2011).

APPENDIX B.1. SOLID TIMBER BEAM CALCULATIONS

NDS for Wood Construction (2017) Method
Solid Timber (1)
Bending Capcaity

Span length	$l = 15\ ft$
Width of specimen	$b = 7.375\ in$
Depth (height) of specimen	$d = 7.25\ in$
Load duration factor (NDS p. 11)	$C_D = 1.25$
Wet service factor (NDS Supplement p. 32)	$C_M = 1.0$
Temperature factor (NDS p. 28)	$C_t = 1.0$
Beam stability factor (NDS p. 15)	$C_L = 1.0$
Size factor (NDS Supplement p. 32)	$C_F = 1.0$
Flat use factor (NDS p.29)	$C_{fu} = 1.0$
Incising factor (NDS p. 29)	$C_i = 1.0$
Repetitive member factor (NDS p. 30)	$C_r = 1.0$
Factor of safety (Desingn of Wood Structures p. 253)	$FS = 2.5$
Reference bending design value for Northern Red Oak Beams, Grade No. 1 (NDS Supplement p. 49)	$F_b = 1350\ psi$

Adjusted bending design value (NDS Table 4.3.1)
$$F_b' = FS \cdot F_b \cdot C_D \cdot C_M \cdot C_t \cdot C_L \cdot C_F \cdot C_{fu} \cdot C_i \cdot C_r = 4219\ psi$$

Allowable Bending Stress
$$\sigma = \frac{M \cdot y}{I}$$

Maximum moment caused by point load at midspan
$$M = \frac{P \cdot l}{4}$$

Depth to neutral axis
$$y = \frac{d}{2} = 3.625\ in$$

Moment of inertia
$$I = \frac{1}{12} \cdot b \cdot d^3 = 234.2\ in^4$$

Maximum allowable point load
$$P_{max} = \frac{4 \cdot I \cdot F_b'}{y \cdot l} = 6057\ lbf$$

Stiffness

Reference modulus of elasticity (NDS Supplement p. 49)
$$E = 1300000\ psi$$

Adjusted modulus of elasticity (NDS Table 4.3.1)
$$E' = E \cdot C_M \cdot C_t \cdot C_i = 1300000\ psi$$

Deflection (AISC p. 3-215)
$$\Delta = \frac{P_{max} \cdot l^3}{48 \cdot E' \cdot I} = 2.42\ in$$

APPENDIX B.2. IBC ALLOWABLE LOAD DERIVATIONS

Derivation of IBC (2018) Allowable Area Load Equation
Mechanically Laminated Decking with Controlled Random Layup
(IBC Table 2306.1.4)

Maximum moment for a three span continuous beam with a uniformly distributed load (AISC Table 3.23: p. 3-227)

$$M_{max} := 0.100 \cdot w \cdot l^2$$

Simplified maximum moment

$$M_{max} := \frac{w \cdot l^2}{10}$$

Generic stress equation for a member in bending

$$\sigma := \frac{M \cdot y}{I}$$

Stress equation with moment of inertia, *I*, and depth to neutral, *y*, axis expanded

$$\sigma := \frac{M \cdot \left(\frac{d}{2}\right)}{\frac{1}{12} \cdot b \cdot d^3}$$

Incorporating the maximum moment into the stress equation

$$\sigma := \frac{6 \cdot w \cdot l^2}{10 \cdot b \cdot d^2}$$

Setting the generic stress equation equal to the adjusted bending design value

$$\sigma := F'_b$$

Distributed load and width are seperated from the rest of the adjusted bending design value equation

$$F'_b := \frac{6 \cdot l^2}{10 \cdot d^2} \cdot \frac{w}{b}$$

Allowable bending stress

$$\sigma_b := \frac{w}{b}$$

Adjusted bending design value equation rearranged to solve for the allowable bending stress

$$\sigma_b := \frac{10}{1} \cdot \frac{F'_b \cdot d^2}{l^2 \cdot 6}$$

Safety factor = 0.66 was applied to to allowable bending stress based on previous research on single span, two span, and three span conditions for laminated decking

$$\sigma_b := 0.66 \cdot \frac{10}{1} \cdot \frac{F'_b \cdot d^2}{l^2 \cdot 6}$$

Simplified allowable bending stress

$$\sigma_b := \frac{6.66}{1} \cdot \frac{F'_b \cdot d^2}{l^2 \cdot 6}$$

Allowable bending stress simplified further to the form presented in the IBC (2018)

$$\sigma_b := \frac{20}{3} \cdot \frac{F'_b \cdot d^2}{l^2 \cdot 6}$$

Derivation of Distributed Point Load Equation Used for Theoretical Predictions

Simply Supported Beam with Single Point Load at Midspan

Maximum moment for a single span beam with a point load at midspan (AISC Table 3.23: p. 3-215)

$$M_{max} := \frac{P \cdot l}{4}$$

Generic stress equation for a member in bending

$$\sigma := \frac{M \cdot y}{I}$$

Generic stress equation with moment of inertia, *I*, and depth to neutral, *y*, axis expanded

$$\sigma := \frac{M \cdot \left(\frac{d}{2}\right)}{\frac{1}{12} \cdot b \cdot d^3}$$

Simplified generic stress equation

$$\sigma := \frac{6 \cdot M}{b \cdot d^2}$$

Incorporating the maximum moment into the stress equation

$$\sigma := \frac{6 \cdot P \cdot l}{4 \cdot b \cdot d^2}$$

Setting the generic stress equation equal to the adjusted bending design value

$$\sigma := F'_b$$

Point load and width are seperated from the rest of the adjusted bending design value equation

$$F'_b := \frac{6 \cdot l}{4 \cdot d^2} \cdot \frac{P}{b}$$

Point load distributed over the width of the member is represented as σ_p to miror the derivation of the IBC (2018) allowable bending stress, σ_b

$$\sigma_p := \frac{P}{b}$$

Adjusted bending design value equation rearranged to solve for the distributed point load, σ_p

$$\sigma_p := \frac{4 \cdot F'_b \cdot d^2}{6 \cdot l}$$

Simplified distributed point load used for theoretical capacity predictions of NLT specimens

$$\sigma_p := \frac{2 \cdot F'_b \cdot d^2}{3 \cdot l}$$

APPENDIX B.3. IBC CALCULATIONS

IBC (2018) Based Method

Dried, Nailed NLT (1)

Bending Capcaity

Span length	$l = 15\ ft$
Width of NLT specimen	$b_{panel} = 8\ in$
NLT depth (height)	$d = 7\ in$
Load duration factor (NDS p. 11)	$C_D = 1.25$
Wet service factor (NDS supplement p. 32)	$C_M = 0.85$
Temperature factor (NDS p. 28)	$C_t = 1.0$
Beam stability factor (NDS p. 15)	$C_L = 1.0$
Size factor (NDS supplement p. 32)	$C_F = 1.2$
Flat use factor (NDS p.29)	$C_{fu} = 1.0$
Incising factor (NDS p. 29)	$C_i = 1.0$
Repetitive member factor (NDS p. 30)	$C_r = 1.15$
Factor of safety (Desing of Wood Structures p. 253)	$FS = 2.5$
Reference bending design value for Northern Red Oak Lumber, Grade No. 1 (NDS Supplement p. 36)	$F_b = 750\ psi$

Adjusted bending design value (NDS Table 4.3.1)

$$F_b' = FS \cdot F_b \cdot C_D \cdot C_M \cdot C_t \cdot C_L \cdot C_F \cdot C_{fu} \cdot C_i \cdot C_r = 2749\ psi$$

Allowable total area load limited by bending (IBC Table 2306.1.4) for a three-span continuous beam

$$\sigma_b = \frac{20 \cdot F_b' \cdot d^2}{3 \cdot l^2 \cdot 6} = 4.62\ psi$$

Allowable distributed point load (Derived from AISC p. 3-215)

$$\sigma_b = \frac{4 \cdot F_b' \cdot d^2}{6 \cdot l} = 499\ \frac{lbf}{in}$$

$$\sigma_b = \frac{P_{max}}{b_{panel}}$$

Maximum allowable point load

$$P_{max} = \frac{2 \cdot b_{panel} \cdot F_b' \cdot d^2}{3 \cdot l} = 3991\ lbf$$

APPENDIX B.4. NLT DESIGN GUIDE CALCULATIONS

NLT Design Guide (2017) Method
Dried, Nailed NLT (1)
Bending Capcaity

Fastener spacing in direction of span (in.)	$s := 7$
Span length	$l := 15\ ft$
Width of NLT specimen	$b_{panel} := 8\ in$
NLT depth (height)	$d := 7\ in$
Load duration factor (NDS p. 11)	$C_D := 1.25$
Wet service factor (NDS supplement p. 32)	$C_M := 0.85$
Temperature factor (NDS p. 28)	$C_t := 1.0$
Beam stability factor (NDS p. 15)	$C_L := 1.0$
Size factor (NDS supplement p. 32)	$C_F := 1.2$
Flat use factor (NDS p.29)	$C_{fu} := 1.0$
Incising factor (NDS p. 29)	$C_i := 1.0$
Repetitive member factor (NDS p. 30)	$C_r := 1.15$
Factor of safety (Desing of Wood Structures p. 253)	$FS := 2.5$
Reference bending design value for Northern Red Oak Lumber, Grade No. 1 (NDS Supplement p. 36)	$F_b := 750\ psi$

Adjusted bending design value (NDS Table 4.3.1)
$$F_b' := FS \cdot F_b \cdot C_D \cdot C_M \cdot C_t \cdot C_L \cdot C_F \cdot C_{fu} \cdot C_i \cdot C_r = 2749\ psi$$

Cross section factor for bending stiffness (NLT Design Guide p. 49)
$$K_{section.b} := 1.0$$

Layup factor for bending strength (NLT Design Guide p. 48)
$$K_{layup.b} := 0.202 \cdot \frac{\left(\frac{l}{d}\right)^{\frac{1}{4}}}{s^{\frac{1}{5}}} = 0.31$$

NLT bending capacity (NLT Design Guide p.50)
$$F_{b.NLT}' := F_b' \cdot K_{layup.b} \cdot K_{section.b} = 847\ psi$$

Allowable bending stress
$$\sigma := \frac{M \cdot y}{I}$$

Maximum moment caused by point load at midspan
$$M := \frac{P \cdot l}{4}$$

Depth to neutral axis
$$y := \frac{d}{2} = 3.5\ in$$

Moment of inertia
$$I := \frac{1}{12}\ b_{panel} \cdot d^3 = 228.7\ in^4$$

Maximum allowable point load
$$P_{max} := \frac{4 \cdot I \cdot F_{b.NLT}'}{y \cdot l} = 1230\ lbf$$

Stiffness

Cross section factor for stiffness (NLT Design Guide p. 49)

$K_{section.E} := 1.0$

Layup factor for stiffness (NLT Design Guide p. 48)

$K_{layup.E} := 0.0436 \cdot \left(\frac{l}{d}\right)^{\frac{9}{10}} \cdot s^{-\frac{1}{5}} = 0.55$

Modulus of elasticity (NDS Table 4A)

$E := 1200000\ psi$

Wet service factor for modulus of elasticity (NDS Supplement p. 32)

$C_M := 0.9$

Adjusted modulus of elasticity (NDS Table 4.3.1)

$E' := E \cdot C_M \cdot C_t \cdot C_i = 1080000\ psi$

NLT modulus of elasticity (NLT Design Guide p. 51)

$E'_{NLT} := E' \cdot K_{layup.E} \cdot K_{section.E} = 592990\ psi$

Deflection (AISC p. 3-215)

$\Delta := \frac{P_{max} \cdot l^3}{48 \cdot E'_{NLT} \cdot I} = 1.10\ in$

APPENDIX C. CRANE MAT COST SUMMARY

All calculations shown in this appendix were done using Mathcad Prime (2011).

Material and Labor Costs

Cost Item	Price ($)	Quantity/Mat	Total ($)
1.25 in. x 7.5 in. x 8 ft piece of lumber	4.68	72	336.96
15 ° Wire Coil Nail	0.013	1440	18.72
R4 Multipurpose Framing Screw	0.10	336	33.60
20 °Jumbo Plastic Strip Scrail	0.11	528	58.08
4 ft Threaded Rod	2.69	4	10.76
Nut and Fender Washer	0.35	8	2.80
Labor Rate for Two People	35.00/hr	3 hr	105.00
Overhead Cost	30.00/hr	3 hr	90.00

Energy Costs

Energy costs were calculated using a commercial electricity rate of 7.836 cents/kWh

Cost Item	Energy Usage (wt)	Time (hrs)/ Mat	Total Energy Usage (kWh)	Total ($)
Electricity to Cut Each Board to Size Using a Table Saw	1000 (1.00 kW)	0.10	0.10	0.01
Electricity to Install Each Nail Using a Nail Gun	1650 (1.65 kW)	0.80	1.32	0.11
Electricity to Install Each Screw Using a Corded Drill	300 (0.30 kW)	0.47	0.14	0.01
Electricity to Install Each Scrail Using a Nail Gun	1650 (1.65 kW)	0.28	0.46	0.04
Electricity to Drill Holes for Threaded Rods Using a Corded Drill	300 (0.30 kW)	0.07	0.02	0.01

Final Disposal Costs

Cost Item	Price ($)	Quantity/Mat	Total ($)
Transportation via Flatbed Truck	3.14/mi	100 mi	314.00
Landfill	48.40/ton	0.75 (1500 lb)	36.30

Total Crane Mat Costs

Mat Type	Total Cost ($)
Nailed NLT Mat	914.66
Screwed NLT Mat	929.44
Scrailed NLT Mat	953.95